Upper and Middle Miocene Ash Beds in the Central Gulf of Mexico

Research Thesis
Submitted in partial fulfillment of the requirements for
graduation with research distinction in Earth Sciences
in the undergraduate colleges of
The Ohio State University

By

Mario Andres Gutierrez
The Ohio State University
2016

Approved by

Dr. Derek E. Sawyer, Advisor
School of Earth Sciences

TABLE OF CONTENTS

ABSTRACT

Volcanic ash beds have been widely used as correlation markers in the Paleogene of the western Gulf of Mexico, but their identification and application as regional events in the Neogene play of the deep water Gulf of Mexico have been underutilized. This study approaches this problem through the organization, identification, and correlation of tuffaceous lithologies, supported by available thin sections, SEM images, biostratigraphy, log analysis, and published studies.

Tuffaceous lithologies can be recognized with great confidence by calibrating sedimentological evidence with petrophysical properties as observed in well logs. Various beds have been encountered in the Miocene of the central Gulf of Mexico, specifically in the Walker Ridge and Green Canyon protraction areas. Direct or semi-direct evidence of amorphous volcanic glass has been documented from petrographic thin-sections, SEM, and XRD analyses. Tuffaceous lithologies have also been described in mud logs of numerous wells. The next best tool to infer ash beds is the spectral gamma-ray log tool, which reveals a distinct increase in thorium content relative to uranium or potassium in both shales and sandstones. An almost unequivocal petrophysical response to the presence of ash beds is the combination of high GR and low bulk density.

Integration of these various lines of evidence within a robust chronostratigraphic framework revealed 11 correlative ash beds in Middle and Late Miocene sandstones and mudstones. Tuffaceous sandstones are preserved in deep-water turbidites and are probably linked to continental ash fall and transport into the Gulf of Mexico. These beds range in thickness from 120 to 250 ft. Tuffaceous mudstones are more likely the result of direct ash fall and preservation in the deep-water environment, and their average thickness is 23 ft. Volcanic activity of the Mid-Late Miocene Yellowstone calderas was the likely source of the volcanic glass found in the tuffaceous lithologies of the central Gulf of Mexico, providing both a long-distance, wind-driven ash fall, and a source-to-sink transport mechanism involving fluvial, deltaic, and deep-water processes. Direct correlation between specific tuffaceous lithologies in the Gulf of Mexico to their specific Yellowstone sources will enhance the Miocene stratigraphic framework of the Gulf of Mexico.

ACKNOWLEDGEMENTS

I would like to thank all the professors, research staff, and fellow students who contributed to my exceptional and outstanding undergraduate experience at the School of Earth Sciences at The Ohio State University. I wish to most sincerely thank my advisor Dr. Derek Sawyer for his guidance, flexibility, time, and encouragement before and throughout the research of this undergraduate thesis. Many thanks to Dr. Larry Krissek, Dr. Wendy Panero, and Dr. Terry Wilson for their fundamental instruction throughout my undergraduate education. The Mayers research scholarship and the Susie L. Shipley Scholarship have served as great supportive resources throughout my studies.

I am thankful to Dr. David Cole for the SEMCAL opportunities and Eagle Ford Shale SURE (Shell Undergraduate Research Experience) experience throughout my undergraduate that defined my scientific foundation and interest for laboratory work. My SURE opportunity was supported by the Shell Exploration and Production Company during the summer of 2013. I am beyond grateful to Dr. Julie Sheets and Dr. Sue Welch for their laboratory expertise and comments on SEMCAL related abstracts/presentations submitted throughout my undergraduate career. Their attentive guidance greatly benefited my scientific and professional development.

An unconditional thank you to my parents Mario Augusto Gutierrez and Elizabeth Diaz for their relentless support and constrictive criticism throughout my undergraduate degree. My sister Sara has been an unmerciful and loving critic of mine since I told her to rebound more at the age of 9. To my paternal grandfather Mario Gutierrez Forero, your strength through all the moments of adversity and emphasis on the value of an education are invaluable. A special thank you to Andrea Cristina Gilson for her sacrifice, patience, and love. I am also very grateful to have the friendships of Angel Guzman and Andrew Burchwell, whose perspective and goodwill provided the balance to the focus. Kobe “The Black Mamba” Bryant also provided an unmatched example of focus and determination.

Finally, the data utilized and interpreted throughout this project were supported by Statoil Gulf Services. I am very grateful to Statoil Gulf Services for the opportunity of the summer 2015 internship and for permission to expand the project into an undergraduate thesis. This project would not be possible without the management and permission of John Oliver. I am especially grateful to Dr. Jose I. Guzman for his mentorship and friendship throughout the internship, and his encouragement to develop my standard of geoscience.

LIST OF FIGURES

LIST OF TABLES

INTRODUCTION

The Gulf Coast of the United States and Gulf of Mexico (GOM) have been a prolific region historically for deep-water hydrocarbon exploration. Volcanic ash beds have been widely utilized as correlation markers through the Paleogene of the Western Gulf of Mexico. The Miocene formations of the prolific Neogene plays of the GOM have not seen extensive use of volcanic paleo makers for framework improvement. Since the 1970's, they have been confirmed in several Pliocene and Pleistocene sandstones reservoirs (Jones, 2008).

Previous studies have approached the presence of volcanic ash in sandstone lithologies with the intention of separating hydrocarbon-holding lithologies from tuffaceous sandstones (Jones, 2008). Typical Direct Hydrocarbon Indicators (DHIs) associated with reservoir sandstones containing low-density hydrocarbons, bounded by deep-water mudrocks, usually present a negative seismic impedance contrast. Similarly, a substantial presence of low density volcanic glass in sandstones can also generate a negative impedance contrast. Further investigation and classification of selected tuffaceous lithologies can lay a vital foundation towards providing a clear contrast between volcanic present sediments, potential false DHIs, and real hydrocarbon indicators in seismic data.

Methods of identification and analysis of ash beds have been previously focused on the provenance and sediment transport processes of the volcanic materials. Previous efforts have concentrated in correlating early Pliocene and Miocene GOM sediments with Yellowstone related sources (Hanan et al., 1998). Figure 1 shows selected continental tuffs that were correlated through laboratory Pb isotope and well logs analysis, and their modeled processes of transport to the GOM. While the precision of age correlation can be improved through the laboratory analysis of Pb isotope signatures of volcanic shards, the cost and proprietary environment of the GOM frequently does not allow for the collection of hard data. In contrast, well logs are a much more common source of data, which contain unique signatures that can support a robust identification of tuffaceous lithologies.

The main objective of this study is to identify, organize, and correlate tuffaceous lithologies in the Miocene in the Central Gulf of Mexico. The petrologic identification and further correlation of ash beds are conducted via the integration of available thin sections, SEM images, biostratigraphy, log analysis, and published studies. The distribution of distinct tuffaceous lithologies in the Central GOM is interpreted through extrapolation of log markers and correlation of similar sedimentary intervals. The correlation of tuffaceous lithologies in the Gulf of Mexico to their specific continental sources will contribute to the understanding of the Miocene stratigraphic framework of the Central GOM.

This project was a part of a geoscience internship at Statoil Gulf Services LLC from May 19th to August 14th of 2015. The featured data that are analyzed specifically for this thesis represent a subset of data permitted for use.

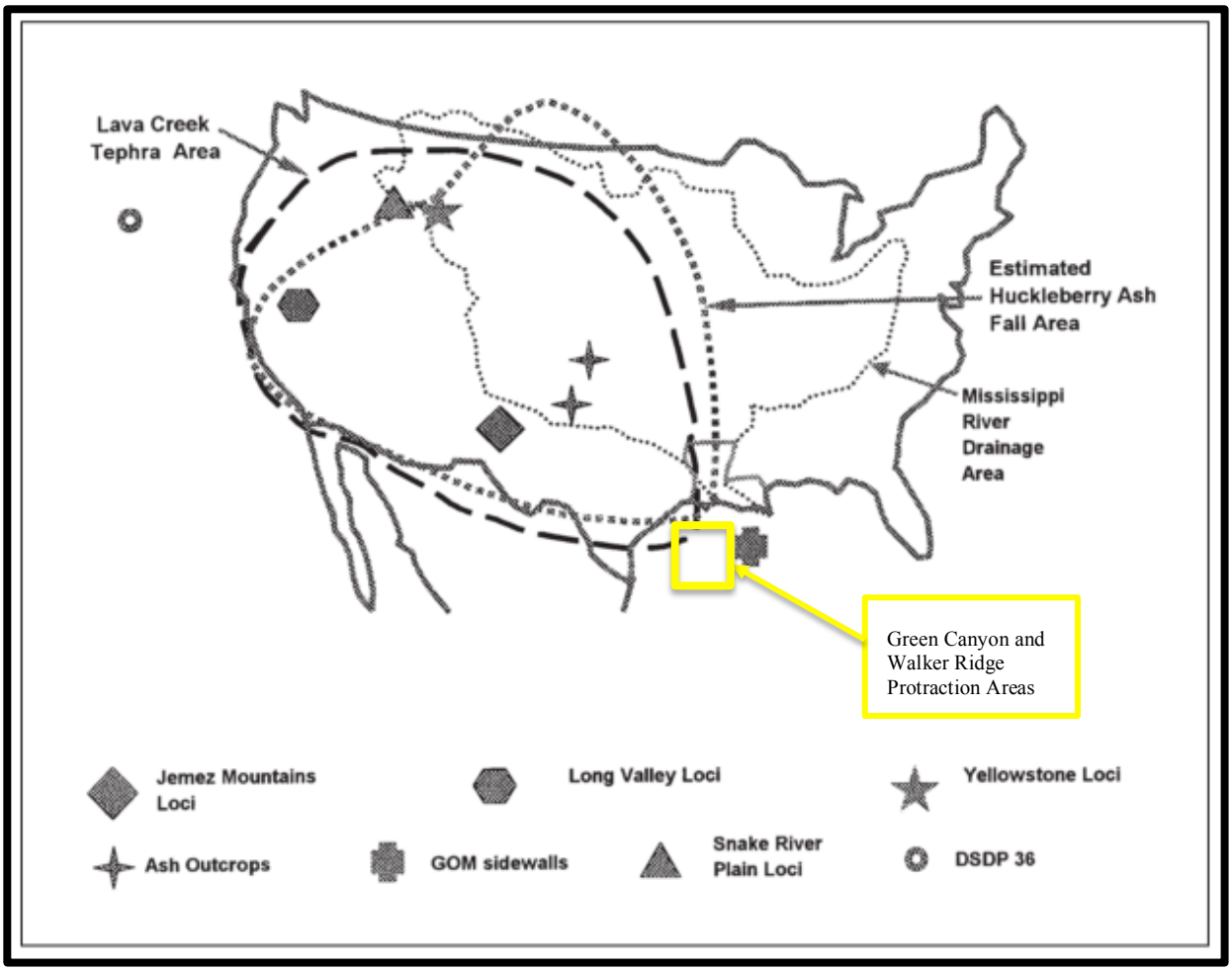

Figure 1. Map of ash fall distribution of eruptions that have been sampled (Hanan et al., 1998).

GEOLOGIC SETTING

Area of Study

The U.S territorial waters of the Gulf of Mexico (GOM) have been extensively studied and explored for hydrocarbons. The U.S government regulates, manages, and leases the development of oil and gas exploration through the Bureau of Ocean Energy Management (http://www.boem.gov/About-BOEM).

The GOM is divided by the regulator into protraction areas. The area of study outlined in yellow includes the protraction areas of Green Canyon and Walker Ridge, which are located in the Western GOM, south of Louisiana (Figure 2). The density of data, economic interest, and lack of previous studies decided the selection of this study area.

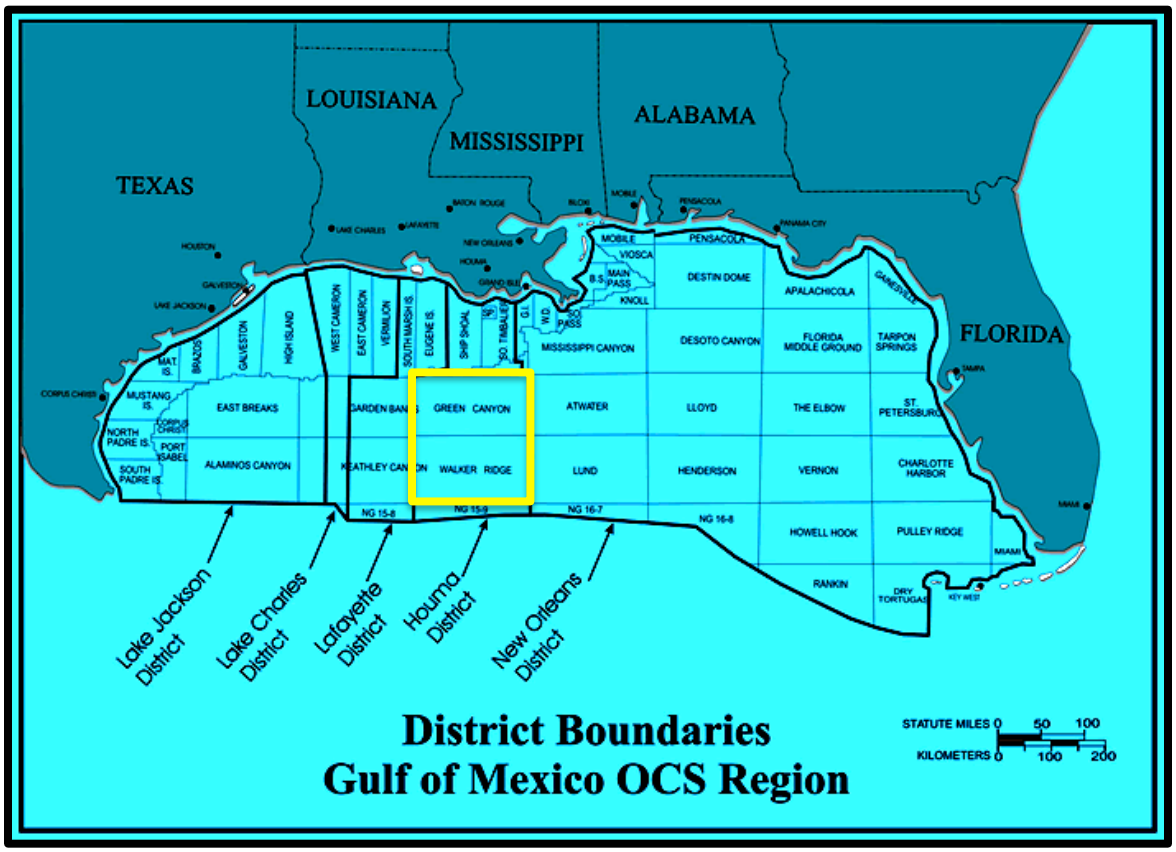

Figure 2. Map of the U.S. Gulf of Mexico. The protraction areas of Green Canyon and Walker Ridge are located in the Houma District. (http://info.drillinginfo.com/offshore-rigs-primer-offshore-drilling/).

Geology

The Gulf of Mexico currently contains a central abyssal plain below more than three kilometers of water depth. The basin was developed through crustal extension throughout the Mesozoic, as it opened during the separation of the North and South American plates. Basement graben and horst development throughout the majority of the Triassic and early Jurassic preceded the main events of rifting that occurred throughout the Late Jurassic and Early Cretaceous (Galloway, 2008). A large deposition of Callovian salt during the Jurassic plays a

vital part of the structural complexity of the basin. Throughout Cenozoic deposition, the Louann Salt detachments impacted the depositional framework of Paleogene and Neogene sediments.

The Gulf basin was insulated from any Laramide orogeny associated sediment due to the Western Interior seaway (Galloway, 2008; Galloway et al., 2011). It was not until the later parts of the Paleocene that continental clastic sediments commenced to enter the basin. This gave way to immense fluvial systems that fed continental margin feeding deltas. Galloway and co-workers (Galloway 2008 and Galloway et al. 2000, 2011) describe the surge and variation of the eight principal sediment depocenters throughout the Cenozoic: Rio Bravo, Rio Grande, Guadalupe, Colorado, Houston-Brazos, Red, Mississippi, and Tennessee (Figure 3).

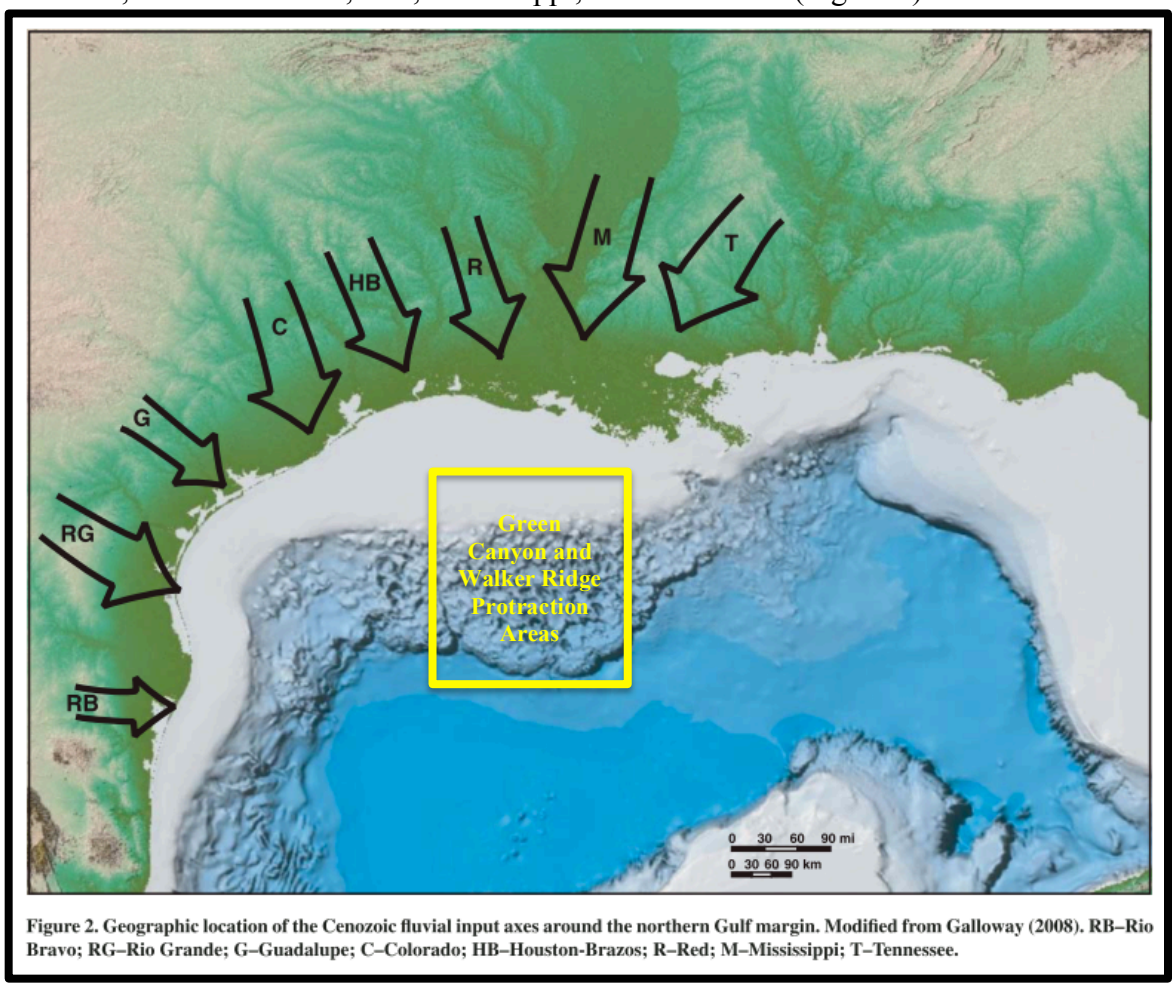

Figure 2. Geographic location of the Cenozoic fluvial input axes around the northern Gulf margin. Modified from Galloway (2008). RB–Rio Bravo; RG–Rio Grande; G–Guadalupe; C–Colorado; HB–Houston-Brazos; R–Red; M–Mississippi; T–Tennessee.

Figure 3. The principal fluvial depocenters throughout the Cenozoic that provided sediment volume to the Gulf of Mexico (Galloway et al., 2011).

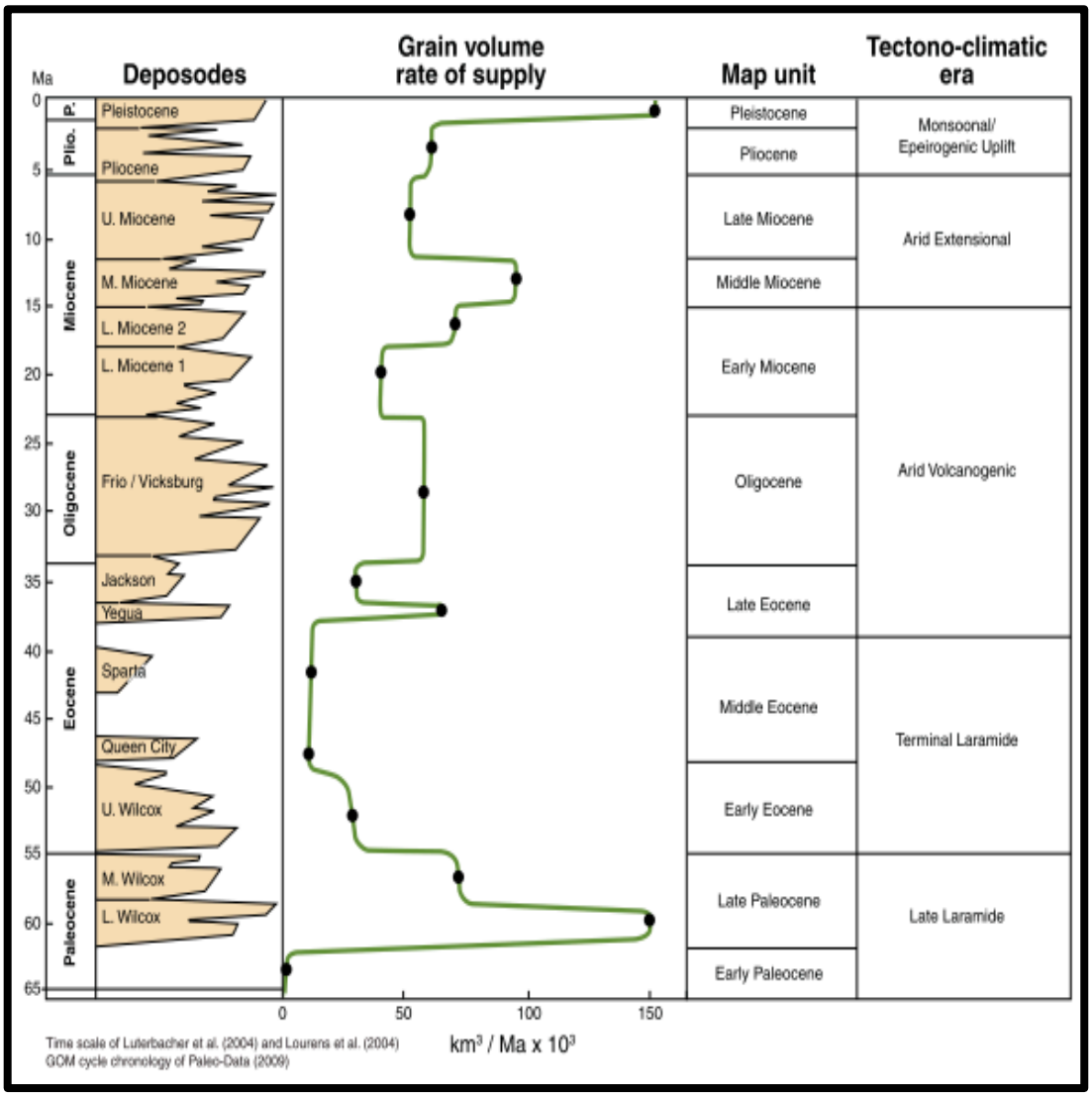

Figure 4. Grain volume in context of depositional episode and the tectonic and climate activity. The graph shows the amount of sediment input throughout time, which is related the magnitude of the fluvial depocenters that developed throughout the Cenozoic (Galloway et al., 2011).

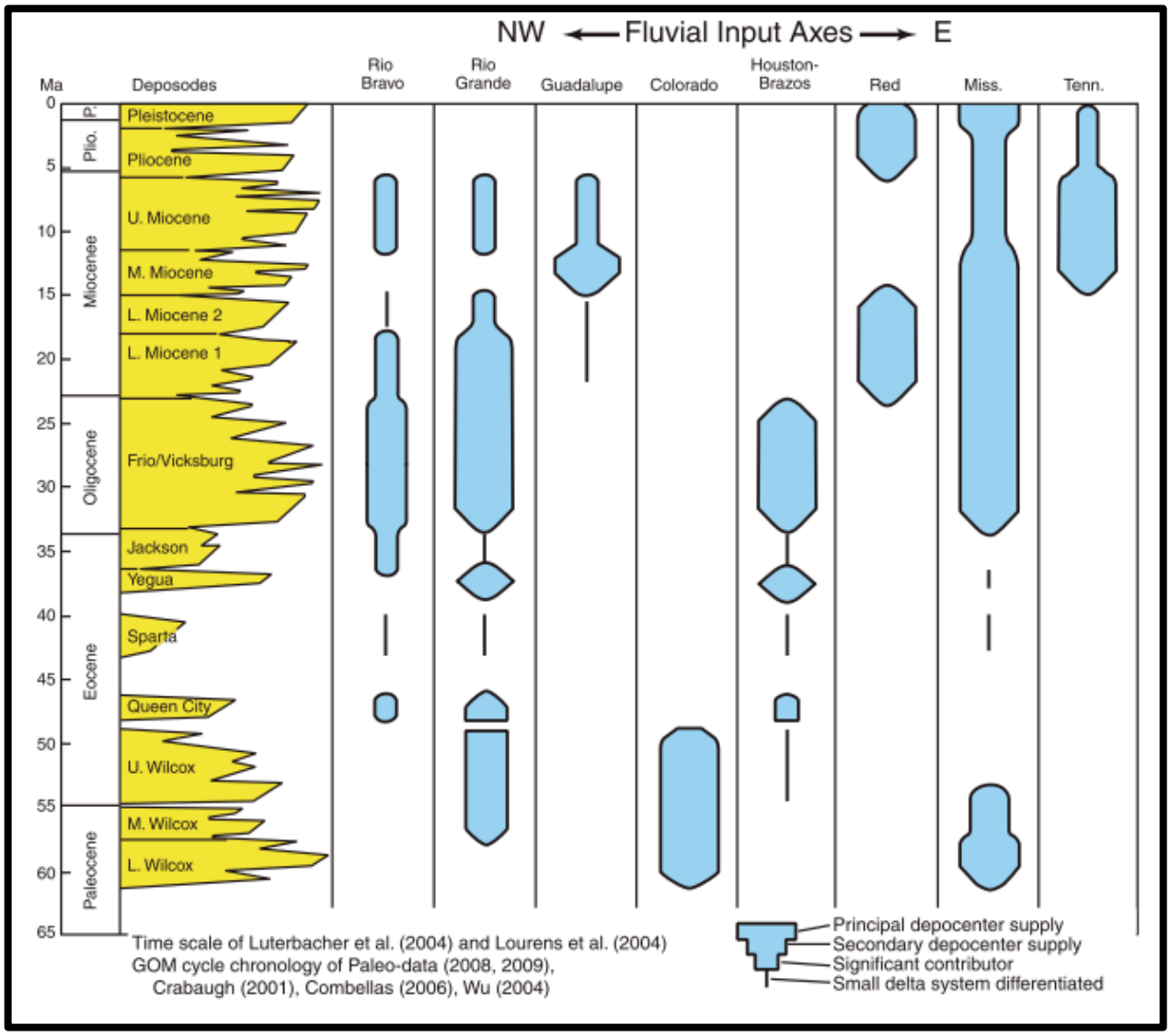

Figure 5. The chart shows the relative importance of depocenter drainage throughout time in relation to the deposodes. It reflects the magnitude of individual depocenters in context of deposodes throughout the Cenozoic. (Galloway et al., 2011)

Depositional History

The following summarized depositional history of the Cenozoic sets the stratigraphic framework for the ashbeds of study and their associated transport processes (Galloway et al., 2011). Entering the late Paleocene, the Colorado and Mississippi paleofluvial systems were established as the principal sediment depocenters. The presence of the Western Interior Seaway and an extended Mississippi drainage basin contributed to a great increase in sediment supply (Figures 4 & 5).

The principal fluvial/deltaic depocenters of the GOM shifted to the Rio Grande and Houston-Brazos rivers during the Early Eocene. Along with this shift, a decline in sediment supply from the western Laramide contributed to several transgressional events in the GOM. The next increase in sediment influx was during the Oligocene, where the Frio/Vicksburg formations received much volume from Mexico and the Southwestern U.S. While the Rio Bravo and the Rio

Grande transported much of the sediment from the Sierra Madre Occidental uplifting, the eastern fluvial/deltaic systems of the Mississippi and Houston-Brazos contributed to a very consistent accumulation that slightly regressed into the Early Miocene (Figure 5).

The Lower Miocene can be characterized mainly by the establishment of the Mississippi fluvial/deltaic system as the principal depocenter contributing sediment to the GOM. The Rio Bravo and Rio Grande systems declined into the Upper Miocene. The Red River system west of the Mississippi received the increase sediment supply from the Mississippi Drainage Basin (Figures 4 & 5). The Middle Miocene introduces the Guadalupe and Tennessee fluvial/deltaic systems, which complemented the main system of the Mississippi River in receiving prominent runoff from the Appalachian uplands and western fluvial systems. The Mississippi fluvial/deltaic system continued to be the dominant depocenter throughout the Upper Miocene, with the Rio Grande and Rio Bravo contributing modestly to the overall sediment supply. The sediment supply due to Rocky Mountain tectonic active along with a decrease of uplift in the Appalachians Mountains contribute to the overall drop off in grain volume into the Gulf.

Continental Volcanic Sources

Throughout the Cenozoic, volcanism was found throughout the western North American Continent. The Laramide Orogeny and Mid-Late Cenozoic tectonically related volcanism are the dominant sources of igneous activity during the development of sedimentary basins. Throughout the Oligocene and the early Miocene, the arid and volcanic tectonic environment of the western continent is characterized by consistent igneous activity such as the Sierra Madre Occidental, San Juan, Basin and Range, and Marysvales volcanic complexes. The Middle and Late Miocene were characterized by the volcanism related to the tectonic extension of the Basin and Range Province. The most active volcanism is concentrated in the Yellowstone Hotspot and Springerville Volcanic Field, and relicts of the Trans Pecos and San Juan volcanic fields (Figure 6).

The Yellowstone hotspot is a series of volcanoes associated with caldera formation through its 434 mile track (Pierce and Morgan, 1992). Named after the Yellowstone Plateau volcanic field, this hotspot started to produce silica-dominated volcanic activity 16.6 Ma (Perkins & Nash, 2002). While currently associated with geothermal activity, the Yellowstone hotspot is regionally traced by numerous tuffs. They are produced by extensive volumes of ash fall and lava flow.

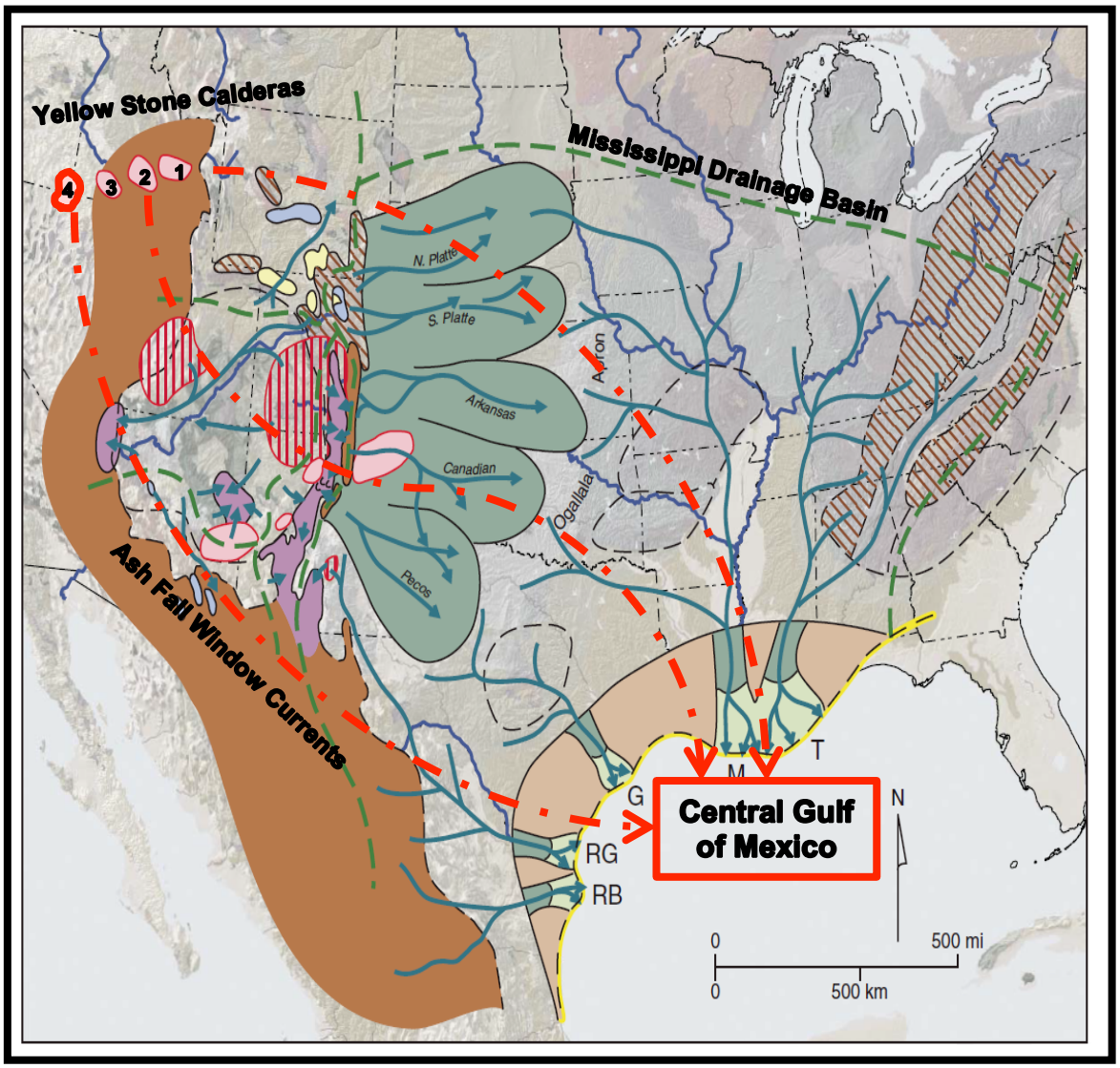

Figure 6. Modified map displays Upper Miocene depocenters, volcanic fields, and fluvial systems of North America (Galloway et al., 2011).

The hotspot is chronologically categorized by different caldera fields that are regionally located along the track to its current location. The different calderas commence at the end of the Burdigalian stage of the Miocene (20.44–15.97 Ma) until current day. Hanan et al. (1998) describe the main four calderas of the middle and early Miocene, including (1) Picabo (10.27–6.5 Ma), (2) Twins Falls (10–8.6 Ma), (3) Bruneau-Jarbidge (12.8–10 Ma), and (4) Owyhee-Humboldt (14–12.8 Ma). Their corresponding number denote their geographic location on Figure 6. Hanan et al.'s studies also correlate early Neogene/Quaternary tuffs, such as the Huckleberry eruption (2 Ma), to the outer continental shelf south of the Mississippi deltaic system (Figure 1). The studies (Hanan et al., 1998) support a depositional model where reworked tuffaceous flows within turbidites are genetically sourced from ash fall within the Mississippi Drainage Basin.

METHODS

Data Inventory

More than 160 wells and related information (well logs, mud logs, paleo data, core, and laboratory analytics) were inventoried for relevant ash present data. An excel spreadsheet database was created to store and track the following factors of ash present wells. Wells were selected based on confidence of identification evidence.

Evidence for Ash Beds

1. Principal evidence

In addition to the immense operational cost environment of the Gulf of Mexico of obtaining a borehole core and/or sidewall cores, the probability of coring an interval of interest with a substantial amount of volcanic ash is very low.

The select amount of petrographic information provides a visual and physical presence of volcanic glass in the dominant lithologies that are identified by mud logs. The shards are characterized by the amorphous, elongated, and angular nature of the grains. The shards contrast sharply against the generally sub-rounded to rounded that characterize a traditional clastic lithology (Petiijohn et al., 1987). The identification of this contrast is confirmed first by thin section analysis and then through petrographic observation of SEM (Scanning Electron Microscope) images.

While rarely available due to cost, Spectral Gamma Ray provides highly accurate information while interpreting ash bed candidates that do not have overwhelming amounts of the previous mentioned evidence. Spectral Gamma Ray individually measures the gamma-emitting components of uranium, thorium, and potassium. The sums of these three components provide the general Gamma Ray measurement (Ellis & Singer, 1989). Radiation emitted from shale sources is potassium, while thorium is the emitting source in ashbeds. The high thorium count explicitly confirms the presence of volcanic glass (Hanan et al., 1998). This is essential in identification when GR is high and RHOB (bulk density) is not consistently low to discount shale.

2. Secondary evidence

Identification of ashbeds is accomplished through a combination of well log signatures. The principal tools that indicate ashbed presence are Gamma Ray (GR), Bulk Density (RHOB), Spontaneous Potential (SP), and Sonic (DTC) (Jones, 2008). While these tools were logged in the Gulf of Mexico, Gamma Ray and Bulk Density were the most commonly logged curves in the study area. Therefore, they are the central focus of well log analysis in this study.

Tuffaceous lithologies and shales have consistently high gamma ray measurements (Hanan et al., 1998). The very low density of volcanic glass discriminates shale when integrating RHOB and GR signatures. This signature of high GR and low RHOB is the most widely utilized type of evidence applied for interpretation throughout this study. This signature has been utilized in previous studies to identify ash beds (Hanan et al., 1998).

3. Supplemental Evidence

Other common logs available are Sonic, Neutron Porosity, Resistivity, and Spontaneous Potential. While these logs do provide indirect information towards ash bed identification, they are not determining indicators. Sonic and SP logs can act as secondary indicating tools, where sonic suggests ash, while SP can discount the possibility of other lithologies (Hanan et al., 1998). Resistivity does not consistently reflect indications of ash. Neutron Porosity detects the presence of hydrogen in a certain lithology, indicating possible hydrocarbon or water. This allows for NPHI logs to be useful in recognizing sandstone rich tuffaceous lithologies, due to a high percentage of bound water (Rider, 2002). Diagenetic alterations of volcanic glass can lead to hydration reaction in clastic dominant lithologies. Alterations of glass and related clays react to zeolites, which contain a high content of water, potentially affecting permeability and porosity (Petiijohn et al., 1987).

Mud logs are a very common source of information that can vaguely provide lithologic information of a well. While it can provide a general confidence of the presence of volcanic sediment, it is very speculative due to the human component of the data collection. The log is representation of examined cuttings, typically in intervals of 10 feet. Precision and accuracy can also suffer to the scope of analysis, where volcanic glass in dominant lithologies can be missed.

Chronologic Orientation through Biostratigraphy

Microfossils and microfauna have essential applications in biostratigraphy and paleo environments. Integrating biostratigraphic information is the next step after developing the evidence criteria and primary identification of ash beds. Distinct biomarkers were organized from well reports correspondingly correlated to biostratigraphic charts (BOEM, Bugware Oil Paleontology, Paleo-Data Inc.) to obtain age brackets for tuffaceous lithologies. The pairs Last-Occurrences biomarkers identify age, and stage, information, providing assurance in the sub-epoch of the particular ashbed.

A first/last occurrence of a microfossil/fauna such as *Discoaster prepentaradiatus* (8.90–10.2 MA) is a principal biomarker of the Upper Miocene in the Gulf of Mexico (Figure 7). *Sphenolithus heteromorphus* (13.53–18 MA) and *Discoaster sanmiguelensis* (12.2–14.5 MA) are staple markers of the Middle Miocene. The microfauna last occurrences (LO) of *Globorotalia mendardii coiling* (5.5 MA) and *Globorotalia foshi perhiperhoacuta* (13.2) occur in the Upper and Middle Miocene. These examples are the principal age constraints of identified ash beds in the Upper and Middle Miocene.

Tuffaceous Lithology Identification Utilizing Well Logs

Well log identification of tuffaceous lithologies is performed on the software platform Petrel 2015, developed by Schlumberger. The software permits correlation, categorization, and mapping of well logs, amongst several other features.

A categorizing nomenclature is established to organize identified lithologies. The sample nomenclature is **ASH_EPOCH_#_A/B**. Epoch specification includes an upper/middle/lower connotation. The numbering starts at the lowest stratigraphically determined interval, increasing in numeration as further intervals are identified up the epoch. **A** signifies the top limit of the interval, and **B** signifies the bottom limit. Tuffaceous lithologies are identified commencing with interpretation of the strongest confidence evidence of individual wells, followed by expanding

extrapolation to other wells through biostratigraphic and well log correlation. Wells from Green Canyon and Walker Ridge are renamed alphabetically to avoid geography of analyzed wells.

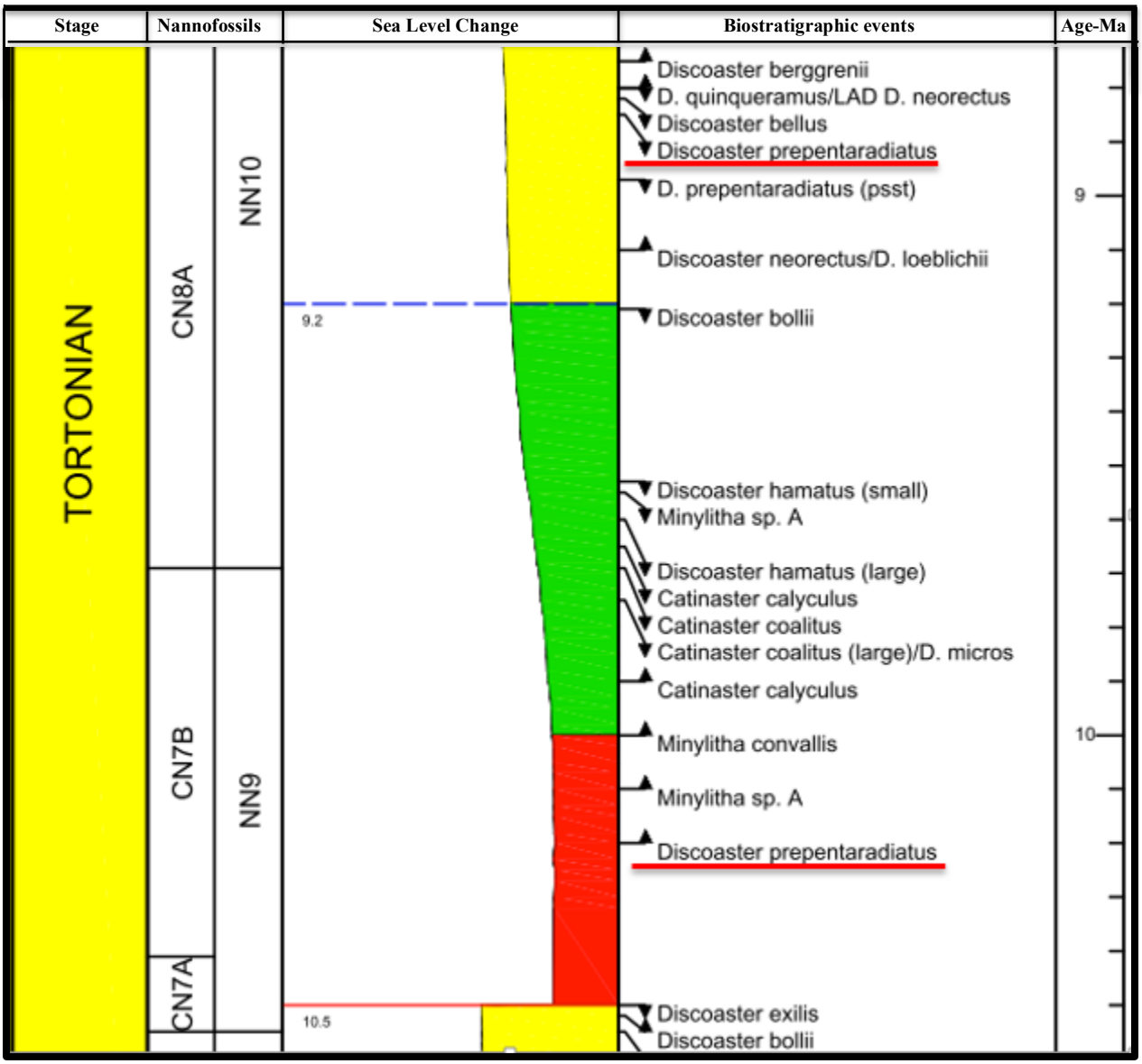

Figure 7. This is an example of utilizing a microfossil (*Discoaster prepentaradiatus*) within a certain biostratigraphic chart to constrain age interval. The first yellow column indicates Stage. The following 2 white columns are nannofossils, followed by the larger column that denotes Sea Level change. The following two columns are the actual biostratigraphic events and age (Ma) of those events (Bugware Inc.).

RESULTS

Of the wells examined, 85 wells contain ash bed indicating evidence; 11 tuffaceous lithologies were identified. Among the wells with ash beds, 37 wells with 4 different tuffaceous intervals were selected for this thesis. The 37 wells were selected as representative of the wells that are permitted for use by Statoil Gulf Services. All wells are within the bounds of protraction areas Walker Ridge and Green Canyon (Figure 2). Biostratigraphic constraints aged 2 intervals to the Upper Miocene and 2 intervals to the Middle Miocene. The log images contain 5 tracks denoted from left to right: GR (Gamma Ray), MD (Measured Depth), RD (Resistivity), Combined NPHI (Neutron Porosity) and RHOB (Bulk Density), and DTC (Sonic). It is very rare to have all tracks present in a certain interval of interest, such as in Figure 8. It lacks the DTC track. The well logs below are representative examples of the total amount of wells interpreted. 8 lithologies are identified in the Upper Miocene and 3 are identified in the Middle Miocene. ASH_MM_1 is the oldest Middle Miocene interval identified. ASH_MM_3 is the 3rd oldest Middle Miocene interval identified. ASH_UM_2 is the 2nd oldest Upper Miocene interval identified. ASH_UM_2 is the 7th oldest Upper Miocene interval identified (Figure 8).

Table 1. Tuffaceous lithologies, age, thickness and wells in which the tuff was identified and the primary lithology of the interval in which the ash was identified.

Ash Bed	Chronostratigraphy	Age (Ma)	Average Thickness (ft)	Number of Wells	Dominant Lithology
Ash_UM_8	Upper Miocene	~5.99	9.33	3	Tuff. Shale
Ash_UM_7	Upper Miocene	~7.7	251.33	9	Tuff. Sandstone
Ash_UM_6	Upper Miocene	~7.7	11	2	Tuff. Shale
Ash_UM_5	Upper Miocene	~9.0	4	1	Tuff. Shale
Ash_UM_4	Upper Miocene	~9.5	10	1	Tuff. Shale
Ash_UM_3	Upper Miocene	~9.5	10	1	Tuff. Shale
Ash_UM_2	Upper Miocene	~10.97	121.45	20	Tuff. Sandstone
Ash_UM_1	Upper Miocene	~10.97	11.5	4	Tuff. Shale
Ash_MM_3	Middle Miocene	~11.7	23.33	3	Tuff. Shale
Ash_MM_2	Middle Miocene	~12.26	22	1	Tuff. Shale
Ash_MM_1	Middle Miocene	~13.68	23.65	17	Tuff. Shale

ASH_MM_1

The oldest interval identified is labeled ASH_MM_1 (Figure 8). This interval is interpreted and correlated in 17 wells, with an average thickness of 23.65 ft. The interval identification is supported by the biostratigraphic presence of LO *Globorotalia foshi peripheroacuta* (identified in 10 of the 17 wells) and LO *Sphenolithus heteromorphus* (identified 14 of the 17 wells). Supplemental data of well reports (10/17 wells), mud logs (14/17 wells), thin section/ SEM petrography (3/17 wells), laboratory analytics (2/17 wells) supported the log curves utilized for interpretation. GR (17/17 wells), Spectral GR (2/17) wells), RD (17/17 wells), RHOB (17/17 wells), NPHI (16/17 wells), DTC (17/17 wells) curves provided the well log measurements to interpret identifying signatures of indicative intervals.

Throughout the well log interpretation, the bottom limit of this interval has a readily identified characteristic, where the peak of the increasing GR throughout the lithology, then immediately kicking left to the baseline value (Figure 9). In Well GC-D, GR approaches 145 API before dropping to the shale base line value of approximately 110 API at 29,287 feet MD. The upper limit of the interval is dictated by a decrease of RHOB from a baseline of approximately 2.65 g/cm^3 to 2.35 g/cm^3. The GR value at the upper limit at 29,274 feet gradually increases from approximately 120 API throughout the interval. The 13 ft interval is clearly identified by the increase of GR, and decrease in RHOB from the over/underlying sands (low GR/RHOB), and shales (high GR/RHOB). The interval in Well GC-F is identified by the gradual increase from the shale baseline of approximately 120 API in GR measurements, combined with a gradual decrease in RHOB from 2.50 g/cm^3 to 2.30 g/cm^3 throughout the 28 ft interval of 28,101 feet– 29,129 feet. The top/bottom limits are not pronounced like GC-D, the overlying and underlying sequences of sands (low GR/RHOB), and shales (high GR/RHOB), provide supplemental assurance in the correlation interpretation.

Well GC-G is identified by GR/RHOB characteristics similar to those of well GC-D. The bottom limit of 29,135 feet is clearly defined by the sharp drop in GR from the interval peak of approximately 145 API to the shale baseline values of approximately 110 API. The top limit of 29,106 feet is clearly shown in the drop of RHOB from approximately 1.50 g/cm^3 to 1.30 g/cm^3 (Figure 10). Well GC-H is identified also by similar top/bottom responses (Figure 10). The bottom limit of 30,386 feet is defined by the sharp drop in GR from 125 API to the shale base line value of 90API. The top limit of 30.371feet is clearly defined by the drop of RHOB from 1.60 g/cm^3 to 1.45 g/cm^3 and back throughout the interval. Correlation of GC-G and GC-H to other wells is supported by the similar GR/RHOB characteristics to GC-D, in addition to the similar large sands and interbedded sequences above/below and similar the interval.

A supplemental characteristic that is specific to ASH_MM_1 throughout all 17 wells and the 4 example wells is the dip in Resistivity (RD). It is not a dependable indicator of tuffaceous lithology; it is a particular characteristic of this specific Middle Miocene tuff. Sonic measurements were not available for this segment of the wells.

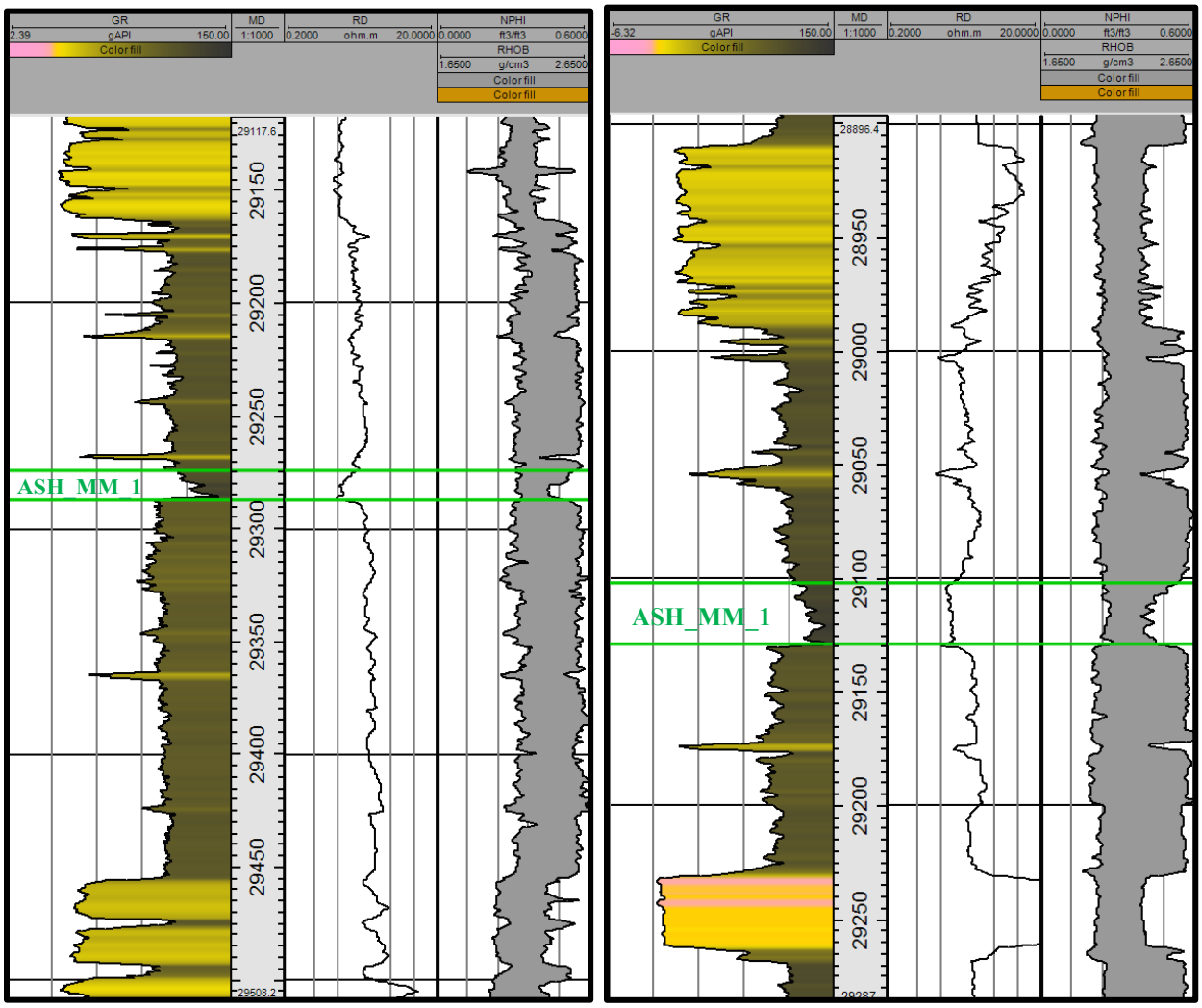

Figure 8. Well logs from GC-D (left) and GC-F (right), light green lines indicate the interval of the tuffaceous lithology ASH_MM_1. It is characterized by high GR, low RD, and low RHOB.

Well GC-D contains a tuffaceous lithologic interval of 13 feet from a depth of 29,274–29,287 feet MD (Figure 8). Well GC-F contains a tuffaceous lithologic interval of 28 feet from a depth of 29,101–29,129 feet MD.

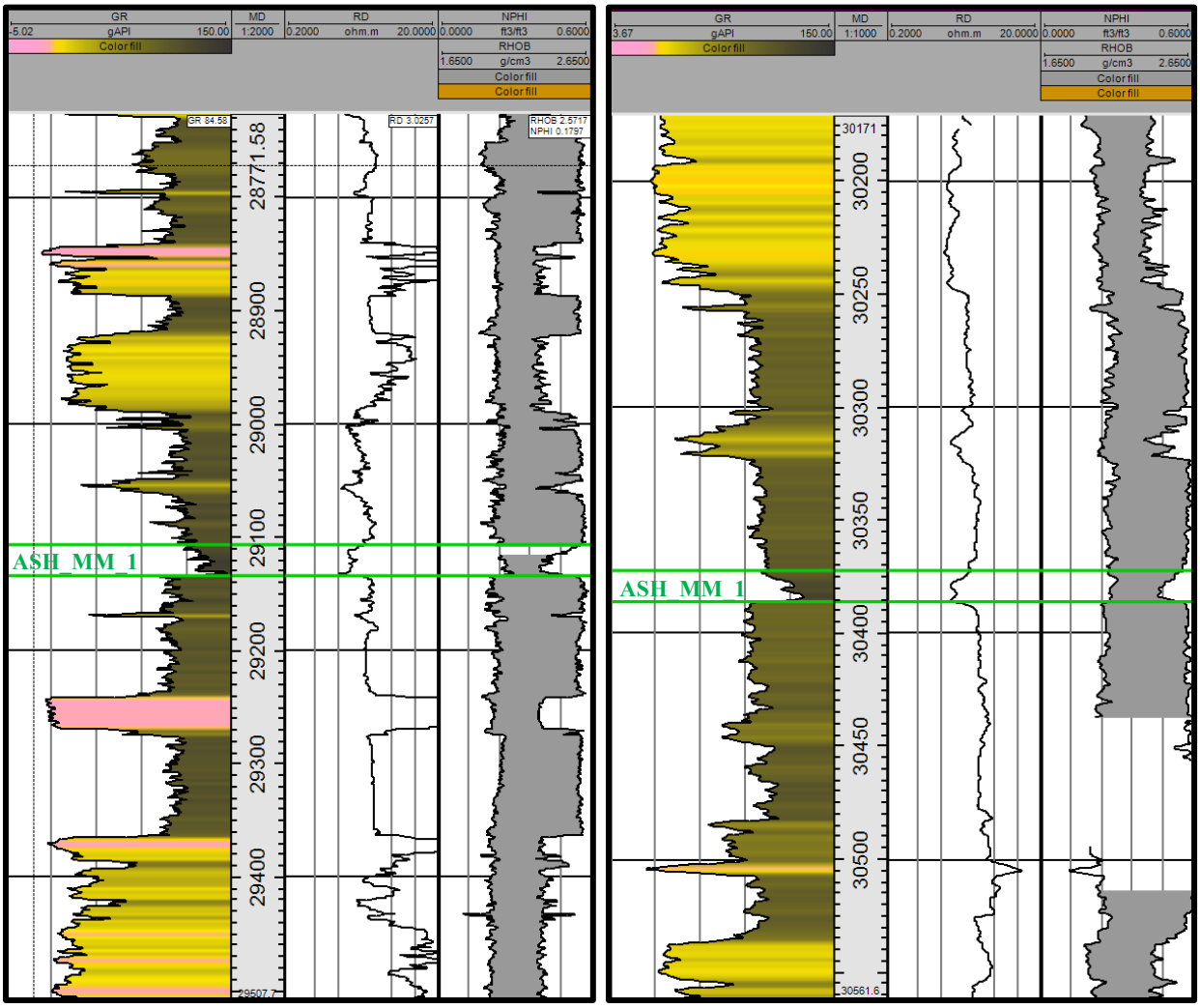

Figure 9. Well logs from GC-G (left) and GC-H (right), light green lines indicate the interval of the tuffaceous lithology ASH_MM_1. It is characterized by high GR, low RD, and low RHOB.

Well GC-G contains a tuffaceous lithologic interval of 29 feet from a depth of 29,106–29,135 feet MD (Figure 9). Well GC-H contains a tuffaceous lithologic interval of 15 feet from a depth of 30,371–30,386 feet MD.

ASH_MM_3

The 3rd oldest interval identified is labeled ASH_MM_3. This interval is present only in 3 wells, providing an average thickness of 23.33 ft (Figure 8). The interval identification is supported by the biostratigraphic presence of LO *Discoaster sanmieguelensis* (identified 2/3 wells) and LO *Coccolithus miopelagicus* (identified 2/3 wells). Supplemental data of well reports (2/3 wells), mud logs (3/3 wells), thin section/ SEM petrography (1/3 wells), laboratory analytics (1/3 wells) supported the log curves utilized for interpretation. GR (3/3 wells), Spectral GR (1/3 wells), RD (3/3 wells), RHOB (3/3 wells), NPHI (3/3 wells), DTC (3/3 wells) curves provided the well log measurements to interpret identifying signatures of indicative intervals.

The high GR, low RHOB signature visually contrasts the interval from overlying and underlying lithologies. The GR in the interval starkly changes from an overlying shale baseline of approximately 120 API to a spike in GR at the top of the interval of 20851 feet. Gamma Ray varies drastically throughout the interval. It is the clear decrease of RHOB from approximately 2.47 g/cm^3 to 2.30 g/cm^3 that suggests this interval as tuffaceous lithology. A particular characteristic of ASH_MM_3 is the interbedded-like fluctuations of GR/RHOB (Figure 11). There are 5 interbedded deep drops in GR to 90–110 API, which correspond with minuscule increases RHOB from 2.45 g/cm^3 to 2.50 g/cm^3. The drops in GR do not decrease enough to solidify the suggestion of a Sandstone lithology, yet the general drop in RHOB discredits indications of clean shale. The measured resistivity does not reflect an identifying characteristic of this interval, and is not an indicator of the presence of volcanic glass. Sonic measurements were not available throughout this segment of the well.

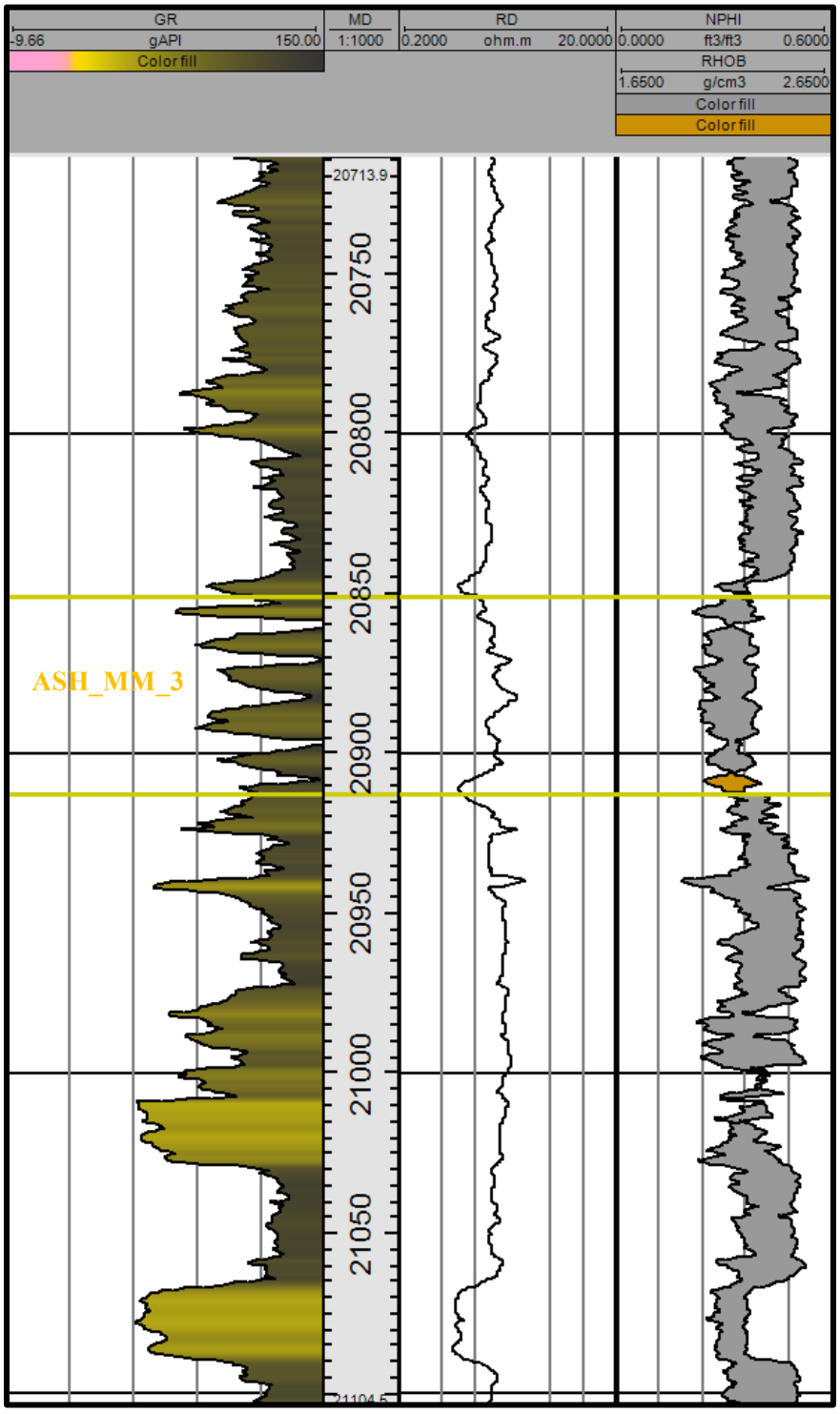

Figure 10. Well logs from WR-Z, yellow lines indicate the interval of the tuffaceous lithology ASH_MM_3. It is characterized by high GR and low RHOB.

Well WR-Z contains a possible tuffaceous lithologic interval of 67 feet from a depth of 20,851–20,918 feet MD (Figure 10).

ASH_UM_2

The 2nd oldest interval in the Upper Miocene identified is labeled ASH_UM_2. This interval is interpreted and correlated throughout 20 wells, with an average thickness of 121.45 Feet (Table 1). The interval identification is supported by the biostratigraphic presence of LO *Discoaster prepentaradiatus* (identified 16/20 wells) and LO *Coccolithus miopelagicus* (identified 13/20 wells). Supplemental data of well reports (14/20 wells), mud logs (15/20 wells), thin section/SEM petrography (6/20 wells), laboratory analytics (5/20 wells) supported the log curves utilized for interpretation. GR (20/20 wells), Spectral GR (5/20 wells), RD (20/20 wells), RHOB (20/20 wells), NPHI (20/20 wells), DTC (20/20 wells) curves provided the well log measurements to interpret identifying signatures of indicative intervals.

ASH_UM_2 varies the most in log signature characteristic and thickness. Well WR- AA represents distinct log measurement characteristics of thick intervals (Figure 11). The limits of the interval are clearly identified by the immediate increase/decrease in GR. The GR curve increases from the shale baseline value of approximately 95–100 API to 130 API at 24,122 feet. The GR value is generally consistent throughout the interval. The gradual and constant dip in RHOB discounts the interval as a shale dominant lithology. The limits of the interval are clearly dictated by sharp changes in log RHOB measurements. The increases in Gamma Ray in those two wells are gradual throughout the interval, while the RHOB measurements visually solidify the identifying signature. Well GC-M is characteristically different in GR/RHOB measurements (Figure 11). The top limit of 21,986 feet is defined by a clear sharp spike in GR from the shale baseline value of 60 API to approximately 90 API, and a sharp drop in RHOB from 1.50 g/cm^3 to 1.20 g/cm^3. The bottom limit is defined by the reserve changes of those values at 22,040 feet.

The bottom limit of Well GC-O is identified by the sharp drop in GR (150 API to shale baseline value 120 API) and the drop in RHOB (1.45 g/cm^3 to 1.25 g/cm^3) at 24,245 feet (Figure 12). The top limit of the interval at 24,209 feet is identified by the general increase in GR from the shale baseline and RHOB. GC-R has RHOB values that decrease from 2.45 g/cm^3 to approximately 2.20 g/cm^3 through the interval. The top and bottom limits are not characteristically sharp as GC-O, but do reflect sufficient change to identify as an ashbed interval.

Both GC-O and GC-R have no indicative resistivity measurement, staying constant throughout ASH_UM_2 (Figure 12). Denoted by the orange fill, RHOB decreases past NPHI in GC-O and GC-M. Wells WR-AA, GC-R and GC-O have similar sequences, with an overlying thin sand that is interbedded within the large compassing shale. The constraints of biostratigraphy in relation to the general lithologic sequences and identifying signatures allowed for correlation of these example wells, and the total 20 wells in interpreting ASH_UM_2 throughout Green Canyon and Walker Ridge.

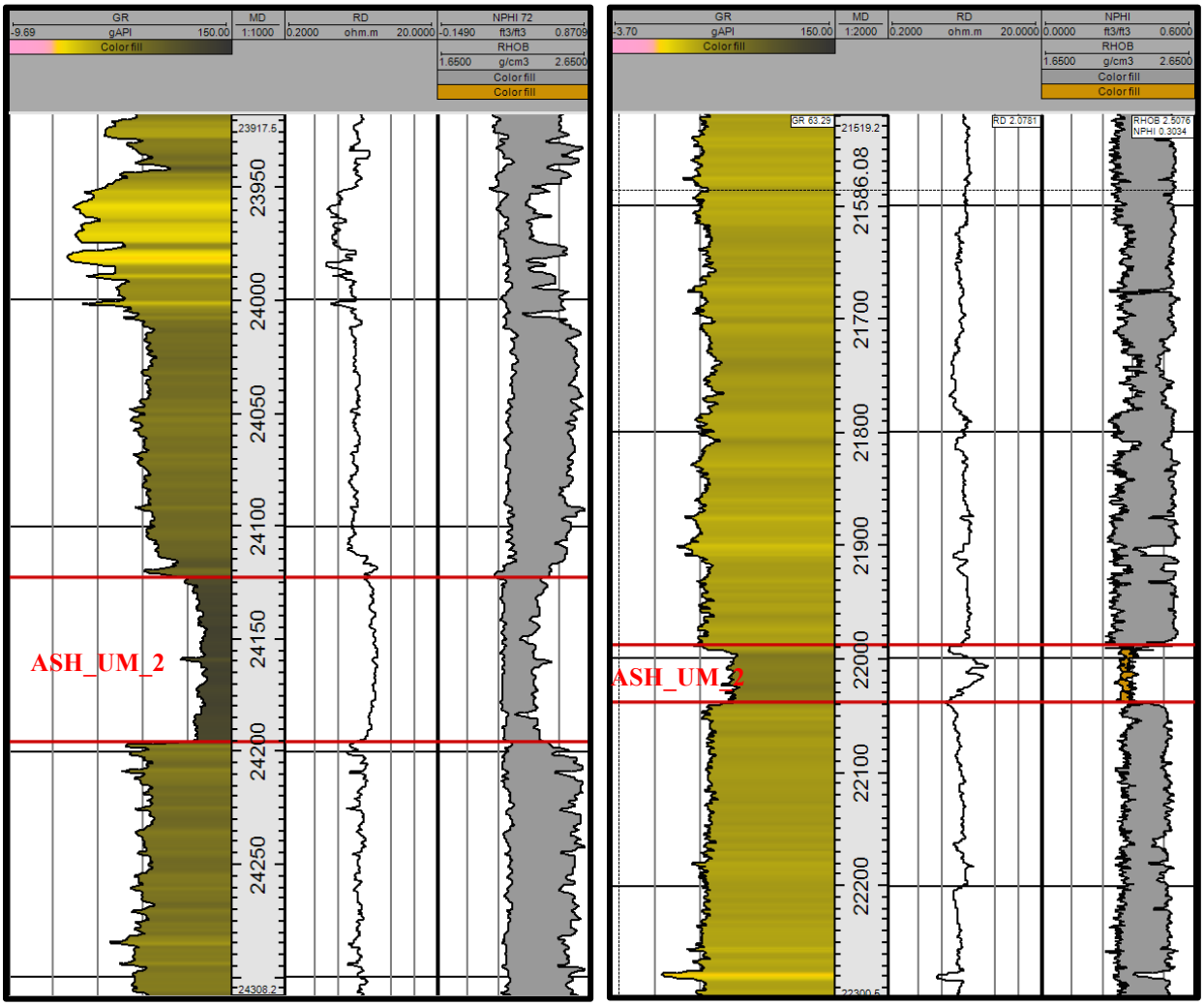

Figure 11. Well logs from WR-AA (left) and GC-M (right), red lines indicate the interval of the tuffaceous lithology ASH_UM_2. It is characterized by high GR, a slight peak in RD, and low RHOB.

Well WR-AA contains a tuffaceous lithologic interval of 73 feet from a depth of 24,122–24,195 feet MD. The well GC-M contains a tuffaceous lithologic interval of 54 feet from a depth of 21,986–22,040 feet MD (Figure 11).

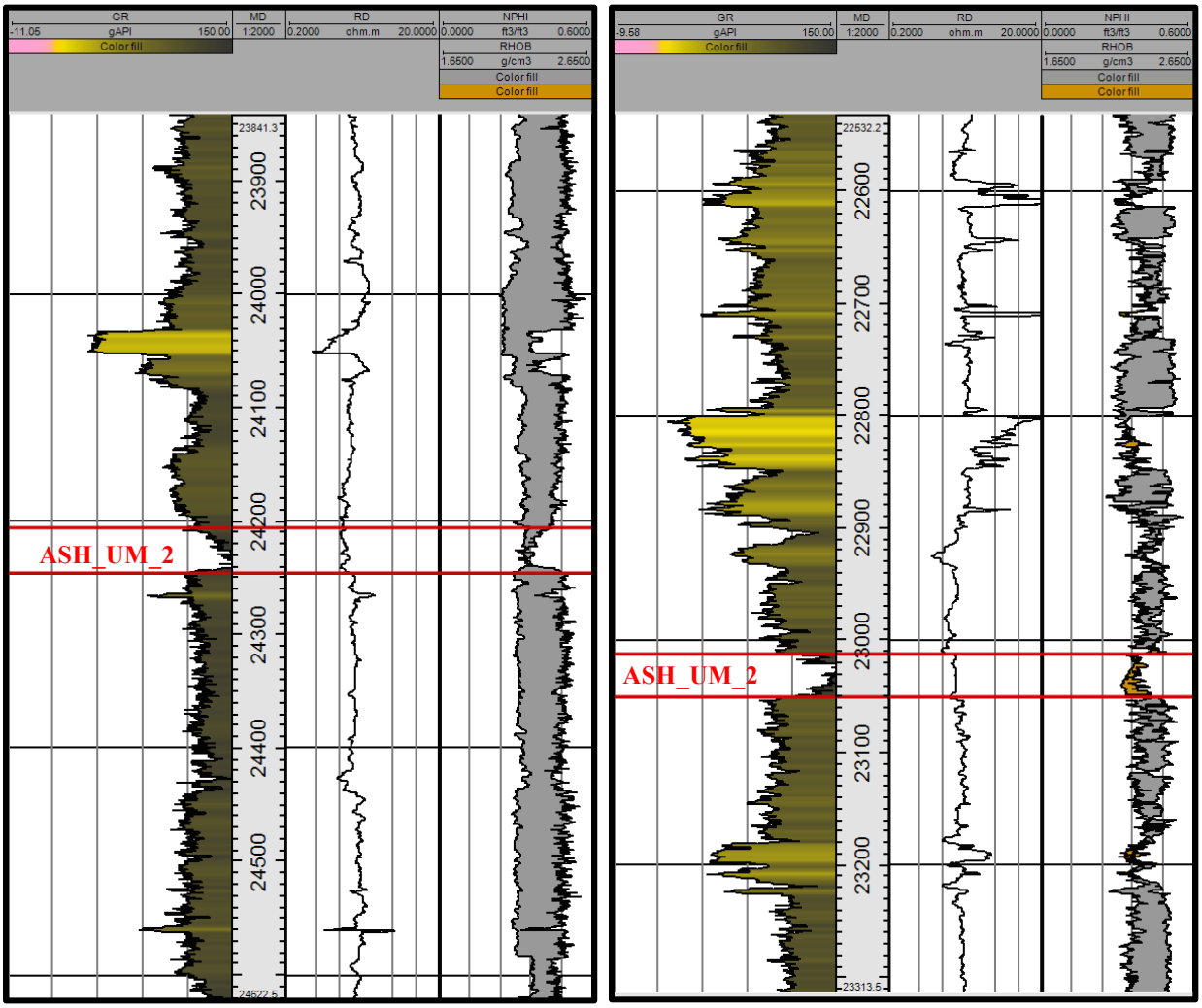

Figure 12. Well logs from GC-O (left) and GC-R (right), light green lines indicate the interval of the tuffaceous lithology ASH_UM_2. It is characterized by high GR, a slight peak in RD, and low RHOB.

Well GC-O contains a tuffaceous lithologic interval of 36 feet from a depth of 24,209–24,245 feet MD. Well GC-R contains a tuffaceous lithologic interval of 37 feet from a depth of 23,013–23,050 feet MD (Figure 12).

ASH_UM_7

The 7th oldest interval in the Upper Miocene identified is labeled ASH_UM_7. This interval is interpreted and correlated throughout 9 wells, with an average thickness of 251.33 feet (Table 1). The interval identification is supported by the biostratigraphic presence of LO *Globorotalia mendardii coiling R/L* (identified 6/9 wells) and LO *Reticulofenestra rotaria* (identified 5/9 wells). Supplemental data of well reports (6/9 wells), mud logs (7/9 wells), thin section/ SEM petrography (2/9 wells), and laboratory analytics (2/9) supported the log curves utilized for interpretation. GR (9/9), Spectral GR (1/9), RD (7/9 wells), RHOB (9/9 wells), NPHI (8/9 wells), DTC (7/9 wells) curves provided the well log measurements to interpret identifying signatures of indicative intervals.

ASH_UM_7 has a large variation in thickness, which is displayed in examples Wells WR-AF and GC-S. Well WR-AF (Figure 13) is the thickness interval of all intervals interpreted, with variations of GR and RHOB. The upper limit of 24,702 feet is principally defined by the readily identifiable sharp decrease in NPHI, complemented by the gradual increase in Gr and low RHOB. Gamma Ray varies throughout the interval, peaking above the shale baseline of approximately 120 API, and decreasing interbeddly throughout. There is an 80 ft package at the bottom of the interval of 60 API with a smaller range between RHOB and NHPI that suggests a coarsening sequence. Well GC-S does not vary so much in the identifying signature (Figure 13). There is a clear change in GR/RHOB at the upper limit of 19,525 feet and lower limit of 19,606 feet. The 81 ft interval reflects 115 API throughout, contrasting the shale baseline values of 80–90 API. RHOB remains at approximately 2.05 g/cm^3 throughout the interval, contrasting from the 2.40 g/cm^3 baseline throughout the imaged sequence.

Well correlation is conducted through the identification of the specific well log signatures of the top/bottom limits of the interval. The constraints of biostratigraphy, the over/underlying sequences allow for correlation of the 2 example wells (total 9 wells) to identify ASH_UM_7.

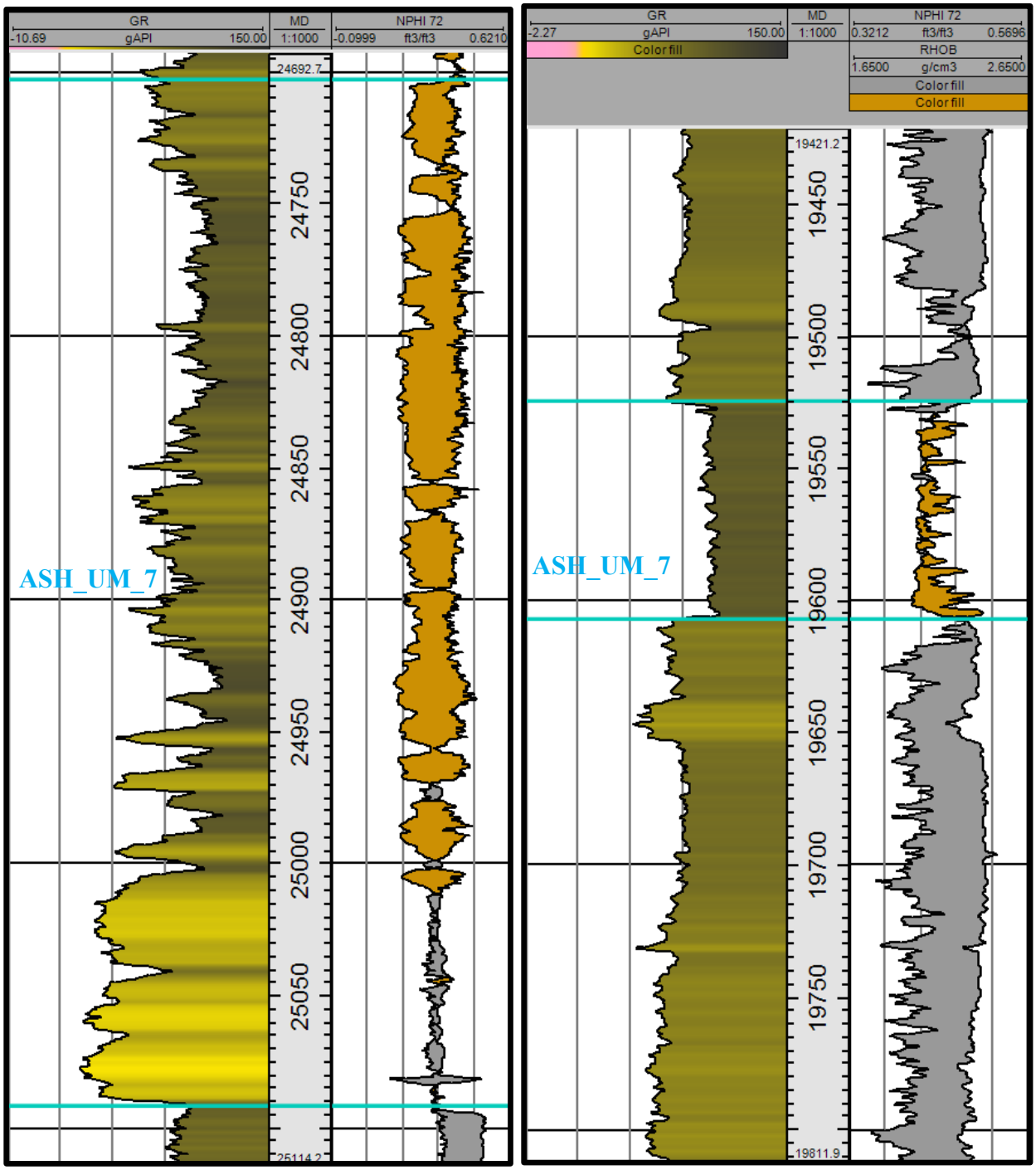

Figure 13. Well logs from WR-AF (left) and GC-S (right), light blue lines indicate the interval of the tuffaceous lithology ASH_UM_7. It is characterized by high GR and low RHOB.

Well log WR-AF contains a tuffaceous lithologic interval of 389 feet from a depth of 24,70–25,091 feet MD. Well log GC-S contains a tuffaceous lithologic interval of 81 feet from a depth of 19,525–19,606 feet MD (Figure 13).

Petrographic Interpretation of Tuffaceous Lithologies

Well log interpretation of the 4 tuffaceous lithologies suggests both shale and sandstone as dominant lithologies. Thin sections, XRD, Grain Count, and SEM Images supplement select intervals. This integration of data solidifies lithologic interpretation of identified intervals. The precise petrologic definitions of associated lithologies are vital in categorizing the ash beds.

Ash is defined as pyroclastic material that is less than 2 mm in size, usually glass shards of rhyolitic composition. A tuff is a lithified ash. When pyroclastic material is deposited by water or wind, such as air fall or turbidite deposits, the lithology is defined as tuffaceous (Petiijohn et al., 1987). Tuffaceous mudstone/sandstone are less than 50% reworked pyroclastic material. A shaley/sandy tuff is considered to contain greater than 50% pyroclastic material (Farooqui et al., 2009). Shale dominant lithologies are deposited by wind currents that deliver air fall deposits far from the source. Clay sized volcanic ash deposits similarly to shale in deep-water environments, and serves as consistent stratigraphic makers (Petiijohn et al., 1987). Sandstone dominant lithologies are most common in alluvial, deltaic, and turbidite deposits, though occurring in all sedimentary environments.

The well log interpretation of ASH_UM_2 and ASH_UM_7 as a sandstone dominant tuffaceous lithology is upheld by petrographic evidence. (Figure 14) The thin section displays evidence of a tuffaceous sandstone mineralogy at 24953 ft throughout ASH_UM_7 in Well WR-AF. The typical mineral contents of a siliciclastic lithology are evident. Subangular quartz grains seen in the thin section are accompanied by smaller grains of feldspar, rock fragments and a grey/green tinted clay and matrix. Elongated, very angular amorphous volcanic glass is present throughout the thin section. This visual evidence of volcanic shards reinforces petrophysical attributes of the well log interpretation of ASH_UM_7. Similar in ASH_UM_2, the well log interpretation of tuffaceous sandstone is refined by visual SEM and bulk mineralogy evidence of a correlated well in Walker Ridge. Figure 15 presents a SEM Image of angular volcanic glass surrounded by different alterations of zeolites and clays. Zeolites are an indication of diagentic alteration of volcanic glass (Petiijohn et al., 1987). The alteration products include different variations of glass, smectite, illite, zeolite and other associated cements. The volcanic glass is coated by spherule and bladed sodium zeolites. Fibrous layers of illite and smectite also surrounded the glass. There is also blocky zeolite cement that reflect late state cement alterations, and lacks clay coating. This visual evidence of volcanic glass is complemented by XRD/Grain Count analysis of the same sample. The pie chart of Figure 16 shows the mineralogic distribution of the sample. Traditional sandstones have less variation in mineralogy than seen here. The amorphous volcanic glass makes up 32.2 % of the composition, cementing the presence of volcanic glass in a sandstone dominant lithology throughout ASH_UM_2. The lithology of ASH_UM_7 and ASH_UM_2 is defined as Tuffaceous Sandstone due to the volcanic material composing less than 50% of the sample mineralogy.

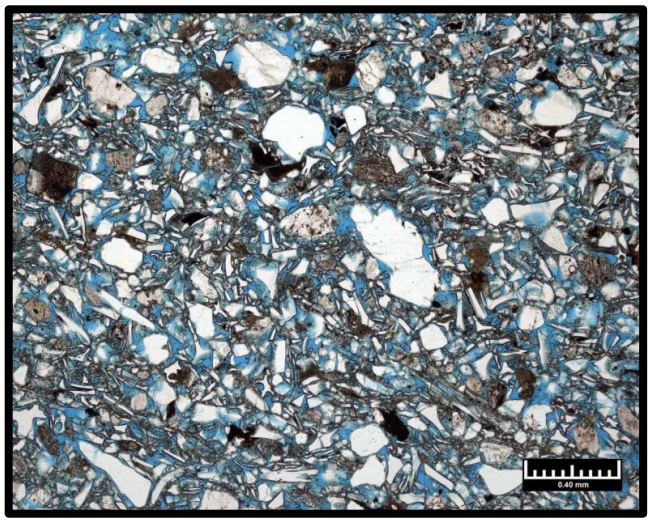

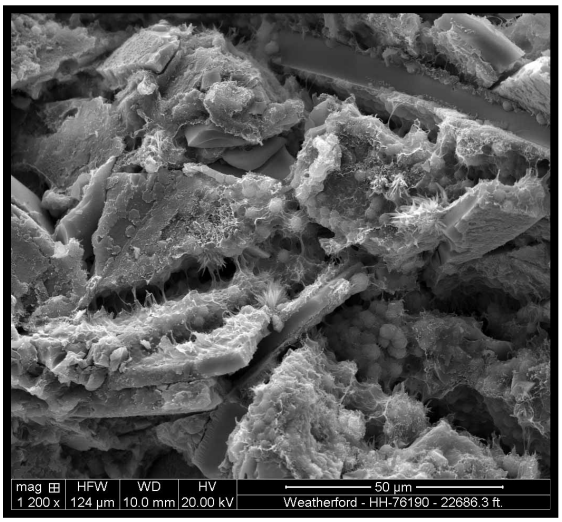

Figure 14. Thin section of sample at 24,953 feet of ASH_UM_7 in Well WR-AF. Figure 15. SEM Image of Well WR-Y of sample correlated to ASH_UM_2.

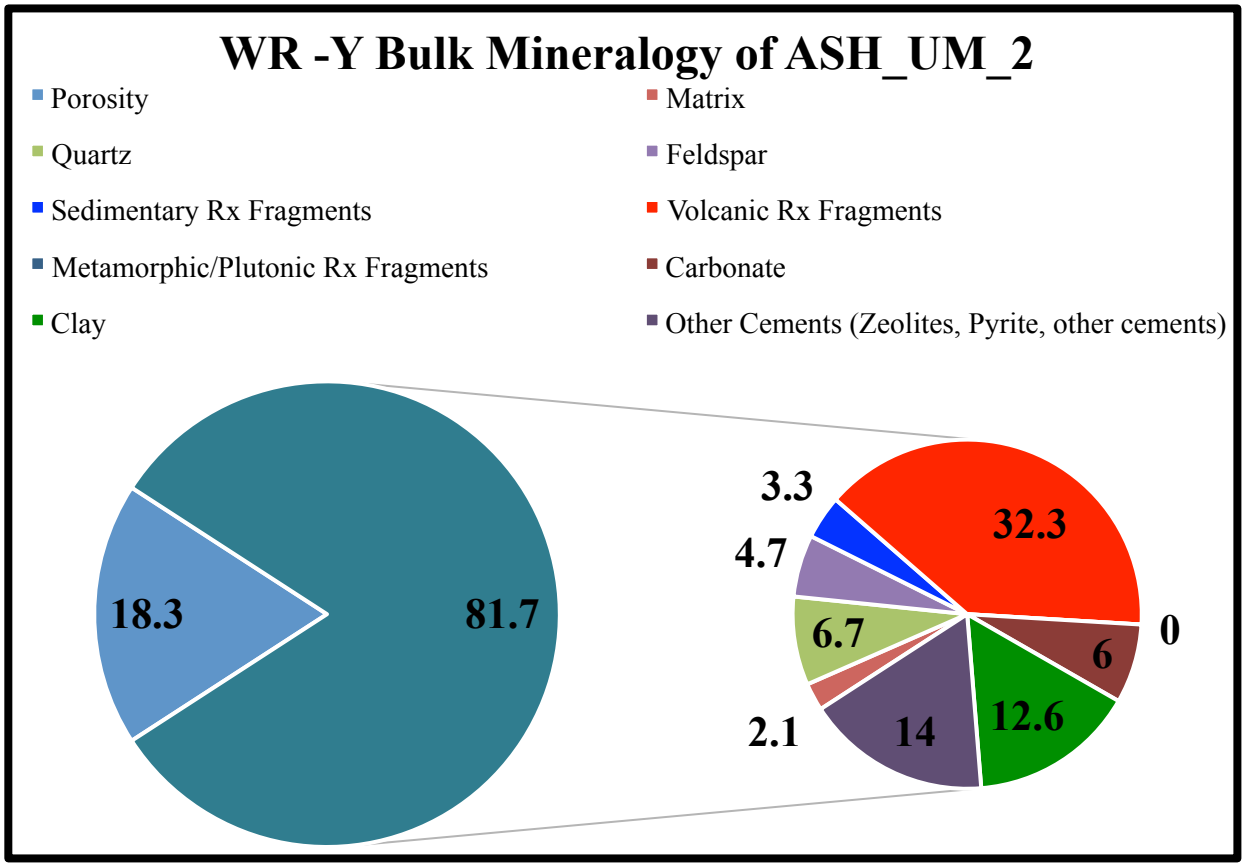

Figure 16. This pie chart proportionally displays the mineralogical contents of the sample in Well WR-Y that is correlated to ASH_UM_2.

The well log interpretation of ASH_MM_1 correlated to dominant shale tuffaceous lithology is upheld by petrographic evidence. A sample collected at 29,115 feet within the

ASH_MM_1 interval of Well GC–F shows a red tinted conchoidal rock, identified as lithified ash, with no indication of other dominant lithology (Figure 17). This visual evidence is integrated further with XRD/Grain Count bulk mineralogy analysis (Figure 18). The volcanic material makes up 54% of the lithology, complemented by 34% of matrix and other minor mineral components. The low porosity of 3%, along with the mineralogical make up and well log interpretation lead to the classification of the lithology of ASH_MM_1 as Tuffaceous Mudstone.

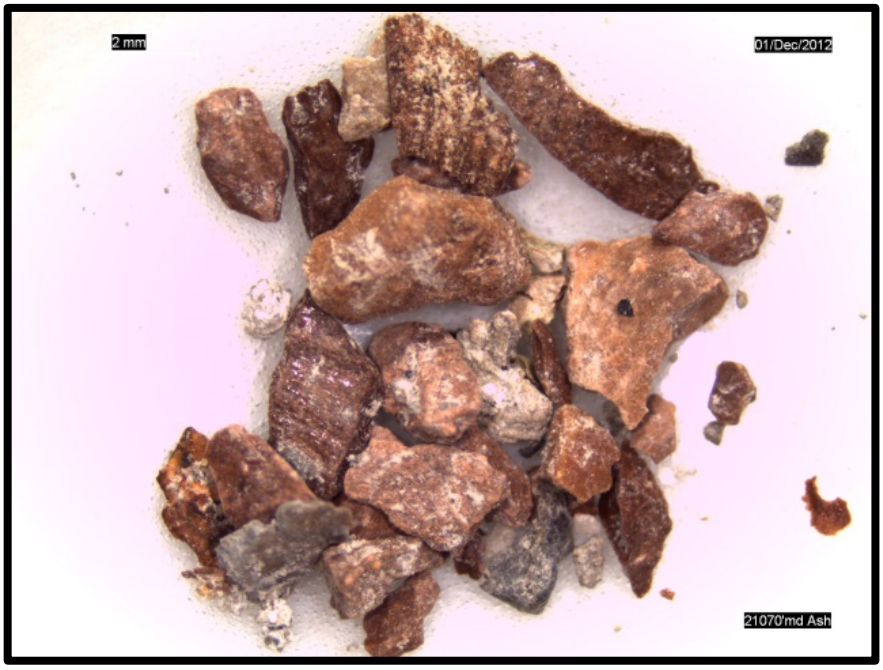

Figure 17. Image of sample ash sample of ASH_MM_ 1 collected at 29115 feet in Well GC-F. The sample imaged is a lithified volcanic ash mudstone.

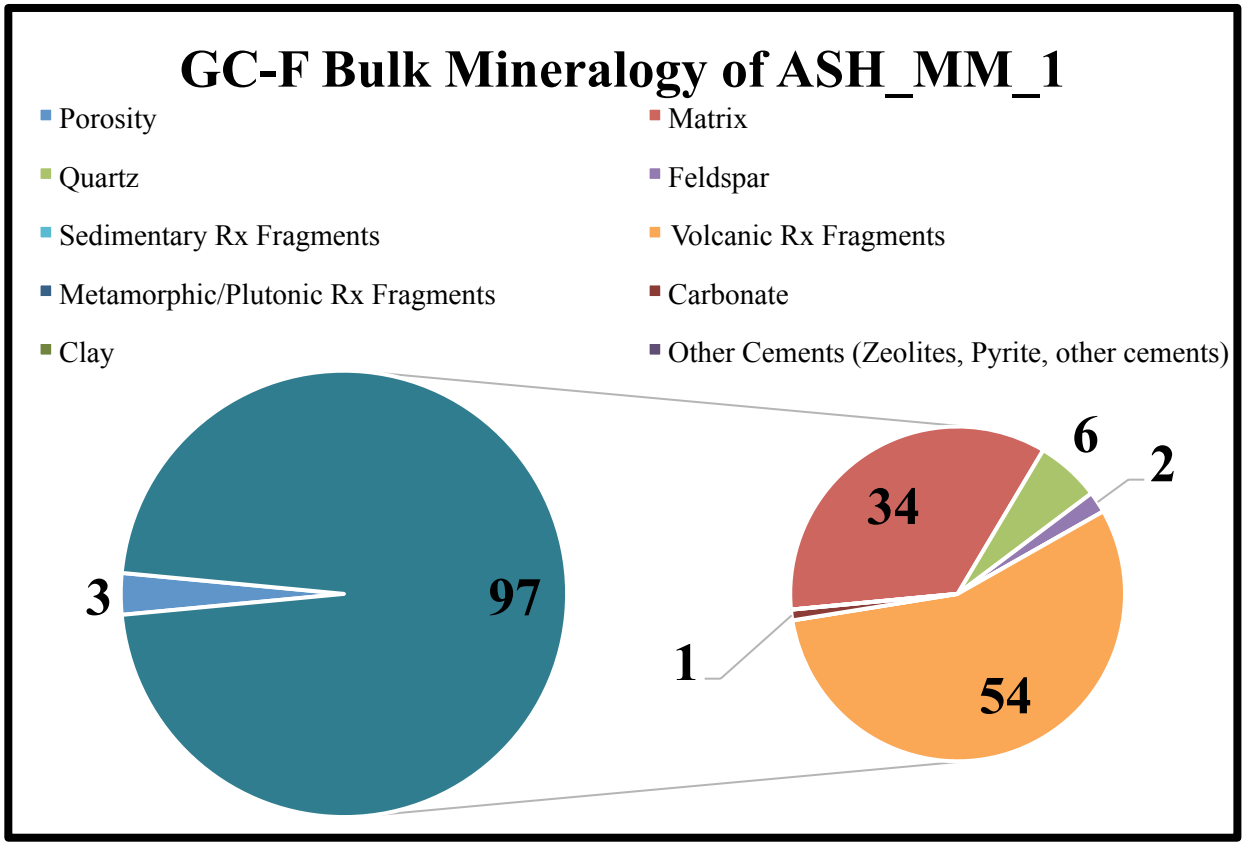

Figure 18. This pie chart proportionally displays the mineralogical contents of the imaged sample at 29115 feet in Well GC-F. It is the bulk mineralogy of the rocks imaged in Figure 18.

The lack of petrologic data leads to the inability to categorize the lithology of ASH_MM_3. The variance in petrophysical measurements within the identification signature did not discount nor cement any dominant lithology.

DISCUSSION

Interpretation of Well Logs with Evidence Criteria

The criteria of a log signature of high GR and a clear decrease of RHOB were very effective in identifying tuffaceous lithologies. The peak in GR is relative to the shale baseline. While the signature is effective and supported by select petrographic evidence of identified intervals, the magnitude of curve measurements depends on the individual intervals. The rare utility of spectral gamma was essential in identification when the primary signature was absent or ineffective. Supplemental logs did not contribute directly to the identification, although certain characteristics of those logs were specific to the ash interval, not to the log interpretation. Mud logs prove to indicate general presence of volcanic glass, but were not sufficient enough to solely identify tuffaceous lithologies.

ASH_MM_1

This interval is interpreted and correlated in 17 wells, with an average thickness of 23.65 ft. The principal indication of categorizing this tuffaceous lithology as a Tuffaceous Shale is the petrologic analysis of the 29,115 ft sample of well GC-F. The visual evidence of the lithified ash and supporting bulk mineralogy (Figure 18) solidify the interpretation of this lithology. The petrologic definition of ASH_MM_1 is extrapolated to the other 3 example wells and 17 total wells of the study through the identification of the signatures of the top/bottom limits of the interval and the sequence of a large sand package underlain by interbedded shales and large shales packages, the tuffaceous interval and then underlain by thin sands. This general sequence is present in the wells, clearly detecting ASH_MM_1.

The evidence of petrology, well log response and average thickness (23.65 feet) that indicate a Tuffaceous Shale are complemented by the small variation of thickness (largest 34 ft, smallest 3 ft) in the wells studied. The small variations of thickness suggest additional indications towards a Tuffaceous Shale. Volcanic ash related to this lithology deposits in suspension similar to shale deposition in deep-water environments. The lithology is not specifically dependent of deep-water turbidite processes, depositing on paleo-topography, and providing the consistent paleo marker that is reflected in ASH_MM_1.

Throughout the constraints of biostratigraphy and integration of previous studies (Hanan et al., 1998), and the depositional attributes associated with ash fall (Petiijohn et al., 1987), this tuffaceous lithology can be tied to the Lower Lobes Tuff of the Owyhee-Humboldt Caldera (Figure 6). This Yellowstone related tuff is aged at approximately 13.80 Ma, correlating to the 13.68 age constraint of ASH_MM_1.

ASH_MM_3

This interval was only present in 3 wells, with an average thickness of 23.33 ft. The lack of petrologic evidence and analysis do not provide any certain indication of petrologic categorization. The well log measurements of ASH_MM_3 in Well WR-Z indicate an interbedded sequence within the interval, but do not suggest any specific dominant lithology (Figure 11). Clear sandstone intervals can be observed below ASH_MM_3, with correspondingly very low GR and low RHOB. Shale baseline defining intervals can be observed above ASH_MM_3. The very high to moderately high API and moderately low RHOB suggest

interbedded shale with a percentage of volcanic glass that alters the wireline measurements from expected shale ranges

Well correlation is extrapolated from the example to the 2 other total wells through the identifying signatures of the top/bottom limits of the interval and the constraints of biostratigraphy. While there is no petrologically clear well log evidence to indicate a dominant lithology, which then would lead to depositional processes, literature suggests the 11.7 MA age of this tuffaceous lithology to the 11.4–12 Ma Tuff of Browns Creek and Tuff of Steer Basin (Hanan et al., 1998). This correlation of tuffs from the Yellowstone related Twin Falls Caldera is based solely on the depositional processes of either direct deep-water ash fall or reworked fluvial/deltaic/turbiditic deposition associated volcanic rich lithologies (Petiijohn et al., 1987). The undetermined dominant lithology of ASH_MM_3 may be correlated to this Yellowstone related source through the age constraints of biostratigraphy and indirect integration of previous literature studies.

ASH_UM_2

This interval is interpreted and correlated throughout the 4 example wells, a total of 20 wells, with an average thickness off 121.45 feet (Figure 8). The principal indications of categorizing this tuffaceous lithology as a Tuffaceous Sandstone are the petrologic analysis of the interval in well WR-Y. The visual evidence of the SEM image (Figure 15) of volcanic glass and associated clays integrated with the bulk mineralogy (Figure 16) of the same sample provide the evident to classify ASH_UM_2 as a Tuffaceous Sandstone. This petrologic definition is extrapolated to the 4 example wells and total 20 wells of the study through well correlation and biostratigraphic support. Well log analyses further support the definition of Tuffaceous Sandstone of the petrologic evidence due to the varying thickness of the intervals. The micro fluctuations of GR/RHOB suggest a variance in percentage of lithology within the dominant sandstone lithology. Thinner beds, such as in GC-O and GC-R share a specific curve character to the identifying log signature.

The large variation in average bed thickness (largest 263 ft, smallest 5 ft) complements the definition of Tuffaceous Sandstone that is solidified by petrologic and well log analysis. Reworked volcanic sandstones are commonly present in most depositional environments. Literature and previous studies connect them to fluvial, deltaic, and turbidity processes (Hanan et al., 1998). These depositional processes do not depend on paleotopography and they may vary throughout deposition (Petiijohn et al., 1987). The thinner beds reside throughout Green Canyon, while Walker Ridge host thicker beds. This observation complements the sediment input of the late Miocene in the Gulf of Mexico, where the principal depocenter of the basin were the intercepting Tennessee and Mississippi depocenters (Figure 5)

As the age constraints of biostratigraphic, well correlation, and integration of literature that associates the reworked volcanic rich lithology with continental ash fall and fluvial/deltaic/turbidity depositional processes (Petiijohn et al., 1987) correlate ASH_UM_2 to an age equivalent Yellowstone continental tuff (Hanan et al., 1998). The 10.97 Ma age constraint of ASH_UM_2 is correlated to the Tuff of Wilson Creek associated with the Twins Falls Caldera (Figure 6)

ASH_UM_7

This interval is interpreted and correlated through 2 example wells and a total of 9 wells of the study, with an average thickness of 251.33 feet. The principal indicators for categorizing this tuffaceous lithology as a Tuffaceous Sandstone are the petrologic analysis of the interval in well WR-AF. The thin section at 24,953 feet provides visual evidence of typical sandstone minerals, with elongated, thin, and angular volcanic shards. (Figure 14) This definition of ASH_UM_7 is extrapolated over a total of 9 wells through specific well log signature identification and biostratigraphic age constraints.

An identifying characteristic of ASH_UM_7 is the signature of RHOB/NPHI throughout the interpreted interval, denoted by the orange fill between the curves (Figure 13). While the thickness and magnitude of GR may vary, Neutron Porosity overlaps Bulk Density in every well analyzed. This observation leads to the association of high water content of altered volcanic glass in the interval, no matter the variations in coarsening or dominant lithology.

The large variance in thickness (largest 426 ft, smallest 9 ft) complements the evidence of a Tuffaceous Sandstone with the depositional implications described for ASH_UM_2. This interval of approximately 7.7 Ma is correlated to the City of Rocks Tuff associated with the Picabo Caldera of the Yellowstone hotspot (Hanan et al., 1998) (Figure 6).

CONCLUSIONS

The principal objective of this study was to identify, categorize, and correlate tuffaceous lithologies in the Miocene in the Central Gulf of Mexico. The establishment of criteria for well log interpretation and integration of biostratigraphic and petrologic data resulted in the clear identification of tuffaceous lithologies in the Middle and Upper Miocene of Walker Ridge and Green Canyon protraction areas. Example intervals of ASH_MM_1, ASH_UM_2, and ASH_UM_7 were interpreted utilizing the identifying signature of GR/RHOB, integrated with thin section, SEM images, and bulk mineralogy data. ASH_UM_2 and ASH_UM_7 are categorized as Tuffaceous Sandstones. ASH_MM_1 is categorized as a Tuffaceous Mudstone. ASH_MM_3 lacked petrologic data and cannot be categorized due to large variances in the identifying signature.

The average thickness of ASH_MM_1 was small in variation. It complements the depositional indicators of ash fall into suspension deposition in deep-water. The large range in the thicknesses of ASH_UM_2 and ASH_UM_7 completed the petrologic and well log evidence that defines the intervals as Tuffaceous Sandstones. Tuffaceous Sandstones are common in all depositional environments, such as those of the sediment depocenters of the Gulf of Mexico in the late Miocene. The 4 tuffaceous lithologies are correlated to Yellowstone related continental tuffs through the integration of literature, sedimentological data, and biostratigraphy.

The study developed methodology of organizing and identifying “ash beds”, and further categorizing the different types of identified intervals. This depth of identification is vital in understanding and improving the stratigraphic framework of the Upper and Middle Miocene of the Gulf of Mexico.

RECOMMENDATIONS FOR FUTURE WORK

The next steps in this study can branch out to several different directions and levels of investigation. One might continue the correlation of already identified lithologies throughout other protraction areas in the region, extending the stratigraphic framework of the Miocene in the Central Gulf of Mexico. Another possible area of investigation is the further application of the developed methodology of well log identification towards other geochronologic time frames and geographic locations.

Further investigation into the continental sources of the volcanic glass would contribute to more knowledge of the provenance and depositional processes of the identified lithologies. Correlations to continental tuffs related to the Yellowstone calderas have been assessed through literature. A future investigation might include isotope dating and field studies to extend previous notions of correlation. Then further investigation into the transportation and depositional processes of individual identified lithologies might be conducted. The integration of paleowind models and further regional paleogeographic information can discount any non-US continental sources and solidify the plausibility of the preliminary notion of the Yellowstone source correlation.

REFERENCES CITED

Ellis, D. V., & Singer, J. M. (1989). *Well logging for Earth Scientists* (2nd ed.). Dordrecht, Holland: Springer.

Farooqui, M. Y., Hou, H., Li, G. et al.. (2009). Evaluating Volcanic Reservoirs. *Oilfield Review*, *21*(1), 36–47.

Galloway, W. E. (2008). *Chapter 15 Depositional Evolution of the Gulf of Mexico Sedimentary Basin*. *The Sedimentary Basins of the United States and Canada* (Vol. 5). The Netherlands: Elsevier. http://doi.org/http://dx.doi.org/10.1016/S1874-5997(08)00015-4

Galloway, W. E., Ganey-Curry, P. E., Li, X., & Buffler, R. T. (2000). Cenozoic Depositional History of The Gulf of Mexico Basin. *AAPG Bulletin*, *84*(11), 1743–1774.

Galloway, W. E., Whiteaker, T. L., & Ganey-Curry, P. (2011). History of Cenozoic North American drainage basin evolution, sediment yield, and accumulation in the Gulf of Mexico basin. *Geosphere*, *7*(4), 938–973. http://doi.org/10.1130/GES00647.1

Hanan, M. A., Totten, M. W., Hanan, B. B., & Kratochovil, T. (1998). Improved Regional Ties to Global Geochronology Using Pb-Isotope Signatures of Volcanic Glass Shards from Deep Water Gulf of Mexico Ash Beds. *Gulf Coast Association of Geological Societies Transactions*, *68*, 2015–2106.

Jones, C. (2008). *Trace Element Fingerprinting in The Gulf of Mexico Volcanic Ash*. Unpublished M.S. thesis, Department of Geology, College of Arts and Sciences, Kansas State University, Manhattan, Kansas.

Perkins, M. E., & Nash, B. P. (2002). Explosive silicic volcanism of the Yellowstone hotspot: The ash fall tuff record. *Bulletin of the Geological Society of America*, *114*(3), 367–381. http://doi.org/10.1130/0016-7606(2002)114<0367:ESVOTY>2.0.CO;2

Petiijohn, F. J., Potter, P. E., & Siever, R. (1987). *Sand and Sandstone 2nd Edition* (2nd ed). Springer Science+Business Media New York. http://doi.org/10.1007/978-1-4612-1066-5

Pierce, K. I., & Morgan, L. A. (1992). The Track of the Yellowstone Hot Spot: Volcanism Faulting, and Uplift. *Geological Society of America Memoir 179*, 1–52.

Rider, M. (2002). *The Geological Interpretation of Well Logs 2nd Ed* (2nd ed). Sutherland, Scotland: Rider-French Consulting Ltd.